

Quantum Critical Paraelectrics and the Casimir Effect in Time

L. Pálová, P. Chandra, P. Coleman

Center for Materials Theory, Department of Physics and Astronomy,

Rutgers University, Piscataway, NJ 08854

(Dated: April 19, 2019)

Abstract

We study the quantum paraelectric-ferroelectric transition with emphasis on observable finite-temperature responses. In the vicinity of the quantum critical point, temperature is a boundary condition in imaginary time that leads to a temporal Casimir effect where critical fluctuations are probed through their sensitivity to external constraints. The resulting finite-size scaling approach yields $\frac{1}{T^2}$ behavior of the paraelectric susceptibility (χ), previously found by other methods, and the scaling form $\chi(\omega, T) = \frac{1}{\omega^2} F(\frac{\omega}{T})$. Self-consistent mean-field theory is used to characterize the classical-quantum crossover in χ , and the resulting temperature-pressure diagram is presented. We also show that coupling to an acoustic phonon at low temperatures influences the transition line and sometimes leads to a reentrant quantum ferroelectric phase. Observable consequences of our approach for high-pressure measurements on specific materials at low temperatures are discussed.

I. INTRODUCTION

The interplay between zero-point fluctuations and boundary conditions leads to the Casimir effect¹, an intrinsically quantum mechanical phenomenon. In recent times, the Casimir phenomenon has assumed a new importance in the design of nanoscale devices². In this paper we show that the effect of finite temperature at a quantum critical point is a temporal analog of the Casimir phenomenon, a “Casimir effect in time”, where temperature imposes temporal constraints on the critical quantum zero-point fluctuations. There is an intimate connection between a finite temporal dimension and a nonzero temperature in a quantum system^{3,4,5,6}, and it has many observable consequences on thermodynamic quantities at nonzero temperatures. Heuristically, this can be understood within the framework of the Heisenberg uncertainty principle where a thermal energy fluctuation leads to a “graininess” in time that is inversely proportional to temperature. More formally within a path integral framework, finite-temperature emerges as a periodic boundary effect in imaginary time; this becomes particularly important near a quantum critical point where there exist quantum fluctuations on all spatial and temporal scales. Here finite-temperature corresponds to the removal of quantum zero-point fluctuations due to the imposition of external constraints, and thus is analogous to the Casimir effect for two parallel metallic plates in vacuum. Running this argument the other way, we note that the removal of temporal modes by periodic finite boundary conditions generates a temperature (and thus entropy and heat) in a system near a quantum critical point. As an aside, we remark that finite-temperature effects resulting from boundary constraints have been discussed in the context of astrophysics where blackbody radiation and event horizons have been linked via the Unruh effect.^{7,8}

In this paper we explore the physical ramifications of temperature as a Casimir effect in time near a quantum ferroelectric critical point (QFCP) where the absence of electronic dissipation, disorder and competing fixed points make this a particularly attractive setting for detailed interplay between theory and experiment. Using finite-size scaling and self-consistent mean-field techniques, we determine the basin of attraction in temperature associated with a QFCP. Exploiting the link between (imaginary) finite-time and nonzero temperature, we calculate measurable thermodynamic response functions of the quantum critical paraelectric and make specific predictions for experiment. We also show that coupling to an acoustic phonon affects the temperature-pressure transition line, sometimes resulting

in a reentrant quantum ferroelectric phase.

At low temperatures the perovskite $SrTiO_3$ (STO) displays a large dielectric response that saturates at $T \sim 4K$; quantum fluctuations are believed to stabilize the paraelectric phase⁹, and this conjecture has been supported by the observation¹⁰ of O^{18} -induced ferroelectricity in STO and by subsequent first-principle studies^{11,12}. It is also known that application of strain, both uniaxial¹³ and epitaxial¹⁴, can induce ferroelectricity. Indeed recent pressure studies of O^{18} -substituted STO indicate that its finite-temperature ferroelectric transition can be tuned continuously¹⁵ to $T = 0$, thereby making it an ideal setting for the detailed study of a quantum critical point¹⁶. More generally over the last decade, there has been a growing interest in the study of large dielectric and piezoelectric responses at cryogenic temperatures.^{17,18} Recent optical studies on isotope-exchanged¹⁹ STO at low temperatures indicate a fascinating interplay between the soft mode and the quantum fluctuations, and this is the central topic of our current study.

Displacive ferroelectrics, particularly those of the uniaxial variety like tetragonal STO, provide familiar settings for the study of critical phenomena. Indeed it was the characterization of the finite-temperature phase transition in uniaxial ferroelectrics, where the upper critical dimension (d_c^u) is three (and thus is experimentally accessible) that led to the first logarithmic corrections²⁰ to mean-field theory in $d = d_c^u$; the subsequent measurement of the predicted specific heat exponent played an important role in establishing the nascent theory of (classical) critical phenomenon²¹. The possibility of a quantum critical displacive transition at zero temperature was also studied using diagrammatic^{22,23}, large- n (component)²⁴ and renormalization-group methods²⁵ and was revisited in a modern framework more recently^{26,27}. Motivated by recent experiment in this area^{16,28}, here we rederive and build upon these results using scaling approaches to quantum critical phenomena with particular emphasis on measurable finite-temperature quantities. More specifically we make predictions for thermodynamic response functions associated with ferroelectrics in the vicinity of the quantum critical point that shed light more generally on the influence of quantum criticality for finite-temperature measurable properties.

We begin with a discussion (Section II) of the Casimir effect in space and time, emphasizing the boundary constraints in each case and noting the mapping between temperature and inverse spatial separation. In Section III we expand on the idea that both the Casimir phenomenon and finite-temperature effects at a quantum critical point (QCP) are

associated with finite-size effects on a system at quantum criticality. We review finite-size scaling in space at a classical phase transition, and then develop its analog in time to derive temperature-dependent quantities near a quantum critical point with specific application to a quantum paraelectric near a QFCP. Self-consistent mean-field theory is used to derive the quantum-classical crossover behavior in χ in Section IV. Coupling between the soft polarization mode and an acoustic phonon is studied in Section V. We show that this leads to a shift in the temperature-pressure transition line and to the possibility of a reentrant quantum ferroelectric phase. We end with a discussion of our results (Section VI) and with everpresent questions to be pursued in future work.

II. THE CASIMIR EFFECT IN SPACE AND IN TIME

The role of temperature at quantum criticality is quite distinct from its role at a classical analogue, where it acts as a tuning parameter $t = T - T_c$ that takes the system through the phase transition. At a quantum critical point other variables, including pressure and doping, play this part. Here temperature, via the thermal energy scale $k_B T$ provides a low energy cut-off for coherent quantum fluctuations; the associated *finite* time-scale is defined through the uncertainty relationship

$$\Delta t \sim \frac{\hbar}{k_B T}. \quad (1)$$

This “graininess” in time manifests itself as a boundary condition in the Feynman path integral; it is in this sense that temperature plays the new role of a *finite-size effect in time* at a quantum critical point^{3,4,5,6}. The interplay between the scale-invariant quantum critical fluctuations and the temporal boundary condition imposed by temperature is reminiscent of the Casimir effect¹, where neutral metallic structures attract each other on micrometer scales^{29,30,31,32} due to zero-point vacuum fluctuations.

In this Section we revisit the ($T = 0$) Casimir effect, reinterpreting it as the response of a (gapless) quantum critical system, the electromagnetic field, to the introduction of spatial boundary conditions that replace a continuum of q-vectors in one direction by a discrete set. This creates a gap in the photon spectrum, causing the Coulomb potential to develop a finite screening length that depends on the plate separation. Analogously we show that, imposing temporal boundary conditions on fluctuations associated with the

quantum ferroelectric critical point (QFCP), we can recover the temperature-dependence of the dielectric response ($\chi(T)$) previously determined by diagrammatic and renormalization-group techniques^{22,23,24,25}. We then proceed to revisit the Casimir effect in space, calculating the relevant sums using the Matsubara method developed for many-body problems at finite temperatures³³; we note that this treatment differs from the conventional derivations^{1,34,35,36,37}, and the analogy between inverse plate separation and temperature emerges naturally here. Later in this paper we will use this mapping to present simple re-derivations of several key properties of paraelectric materials in the vicinity of a QFCP. As an aside, we note that the Casimir effect has been invoked to support the maritime tale that rolling ships attract one another on short distances³⁸, so we are not the first to generalize Casimir's ideas beyond their original setting.

In Figure 1 we present a visual comparison of the Casimir effect in space and time. In both cases the finite boundary effects induce the replacement of a continuum of quantum mechanical modes by a discrete spectrum of excitations, and there are very close similarities between the path integral expressions for the underlying quantum dynamics. Here we consider the conventional Casimir effect with parallel boundary-plane geometry.

The matrix element of the time-evolution operator $U(\bar{t}) = e^{-iH\bar{t}/\hbar}$ in the Casimir effect is represented by a Feynman path integral

$$\langle U(\bar{t}) \rangle = \langle \psi_0 | e^{-i\frac{H\bar{t}}{\hbar}} | \psi_0 \rangle = \int_{Paths} \exp \left[i \frac{S[E, B]}{\hbar} \right] \quad (2)$$

where $S[E, B]$ is the classical action of the electromagnetic field

$$S = \int_{-\bar{t}/2}^{\bar{t}/2} dt \int_0^a dz \int d^2x \left[\frac{\epsilon_0 E^2}{2} - \frac{B^2}{2\mu_0} \right] \quad (3)$$

and the final time \bar{t} is to be taken to infinity at the end of the calculation. The important point here is that the spatial integral runs over $z \in [0, a]$ so that the modes inside the path integral involve zero-point fluctuations of electromagnetic field modes of the form

$$\vec{E}(\vec{x}, z) = \sum_{\vec{k}, n} \vec{E}_{\vec{k}n} e^{i\vec{q}_\perp \cdot \vec{x}} \sin \left(\frac{n\pi}{a} z \right) \quad (4)$$

where $\vec{E}_{\vec{k}n}$ is the Fourier amplitude of the field and \vec{x} is the position co-ordinate parallel to the plates. The Fourier modes of these fluctuations involve a discrete set of wavevectors,

$$\vec{q}_n = (\vec{q}_\perp, q_{zn}), \quad (n > 0) \quad (5)$$

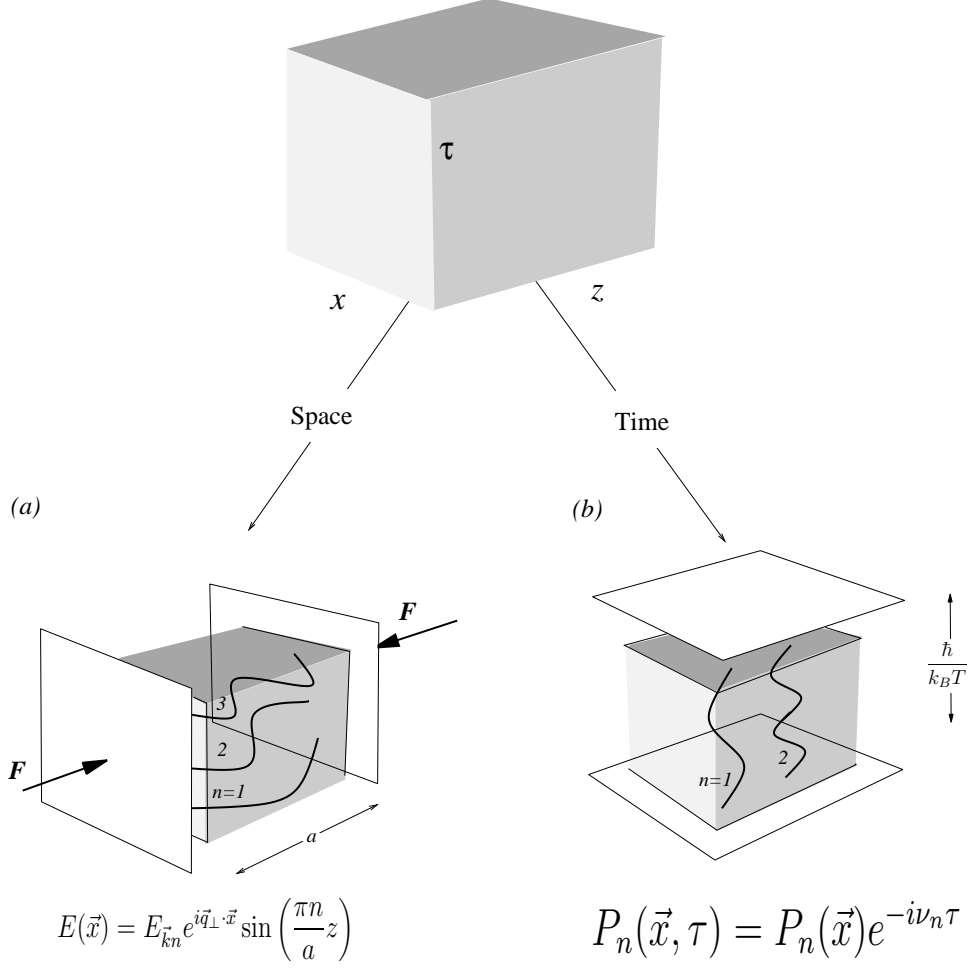


Figure 1: Casimir effect in space and time. (a) Imposition of spatial boundaries on the quantum critical electromagnetic field yields the conventional Casimir effect (b) Imposition of temporal boundary conditions on a quantum critical paraelectric generates the effect of non-zero temperature.

where $q_{zn} = n \left(\frac{\pi}{a}\right)$, leading to a discrete set of normal mode frequencies $\omega_{\vec{q}_\perp n} = c\sqrt{\vec{q}_\perp^2 + q_{zn}^2}$.

The Casimir effect results from the removal of zero-point fluctuation modes from a gapless field. The associated energy is the *finite* difference between the zero-point energies with and without the plates^{1,34,35,36}. The zero-point energy of the fields inside the plates is given by

$$E_C = 2 \sum_{\vec{q}_\perp, n > 0} \frac{\hbar \omega_{\vec{q}_\perp, n}}{2} = A \quad (\hbar c) \sum_{n > 0} \int \frac{d^2 q_\perp}{(2\pi)^2} \sqrt{q_\perp^2 + q_{zn}^2}, \quad (6)$$

where the prefactor accounts for the two light polarizations and A is the area of the plates. The quantity $\frac{E_C}{A}$ determined from (6) is dimensionally of the form $[E_C/A] = \hbar c [L^{-3}]$. Since a is the only length-scale in the system, it follows that the change in the zero point energy

must have the form

$$\frac{\Delta E_c}{A} = -\mathcal{C} \frac{\hbar c}{a^3}, \quad (7)$$

where the sign is chosen in anticipation that the loss of modes reduces the zero-point energy. The fact that the Casimir energy is sensitive to arbitrary interplate separation, a , is a direct consequence of the gaplessness, and thus scale-free nature, of the photon field. In standard derivations, the constant $\mathcal{C} = \frac{\pi^2}{720}$ is calculated using regularization methods with imposed cutoffs that are subsequently removed^{1,34,35,36}. We will shortly present an alternative derivation where the link to finite-temperature physics emerges naturally.

Table. 1. Casimir Effect and Quantum Criticality.

	Casimir Effect	Quantum Criticality
Boundary condition	Space	Time
“S matrix”	$U = e^{-iE\bar{t}/\hbar}$	$Z = e^{-\beta F}$
Path Integral	$U = \int D[\phi] \exp \left[i \frac{S[\phi]}{\hbar} \right]$	$Z = \int D[P] \exp \left[-\frac{S_E[P]}{\hbar} \right]$
Action/time	E	$\frac{S_E}{\beta\hbar} = F$
Time interval	$\bar{t}(\rightarrow \infty)$	$\beta\hbar$
Spatial interval	a	∞
Discrete wavevector/frequency	$q_{zn} = \left(\frac{\pi}{a}\right) n$	$\nu_n = \left(\frac{2\pi k_B T}{\hbar}\right) n$

The Casimir effect is thus a boundary condition response of the electromagnetic vacuum. The gapless nature of the photon spectrum means that the zero-point electromagnetic fluctuations are scale-invariant; the vacuum is literally in a quantum critical state. However, once the boundary conditions are introduced, the system is tuned away from criticality and develops a finite correlation length. In particular the Coulomb interaction between two charges, the correlation function of the electromagnetic potential inside the cavity, is changed from

the vacuum to the cavity as

$$V(q)_{free} \sim \langle \delta\phi_q \delta\phi_{-q} \rangle = \frac{e^2}{q^2} \quad \rightarrow \quad V(q)_{cavity} \sim \frac{e^2}{q_{\perp}^2 + \xi^{-2}} \quad \xi = \frac{a}{\pi} \quad (8)$$

where the plates have removed field modes and have introduced a finite correlation length ξ .

In a closely analogous way, the partition function of a quantum system at finite temperatures is described by a Feynman path integral over the configurations of the fields in Euclidean space-time³⁹, that is, the configurations in space and *imaginary time* τ . We recall that the link between statistical mechanics and quantum physics in imaginary time is accomplished by noting that the Boltzmann density matrix $\hat{\rho}(\beta) = \exp[-\beta\hat{H}]$ is equal to the Heisenberg unitary time evolution operator $\hat{U}(t) = \exp[-\frac{it}{\hbar}\hat{H}]$ evaluated at an imaginary time $t = -i\hbar\beta$,

$$\hat{\rho}(\beta) = \hat{U}(-i\hbar\beta) \quad (9)$$

so that the partition function

$$Z = \text{Tr} \left[e^{-\beta H} \right] = \text{Tr} [U(-i\hbar\beta)] \quad (10)$$

is then computed using a unitary time evolution operator (in imaginary time). This operator trace is then transformed using coherent states into a path integral formulation.

In the quantum paraelectric of interest in this paper, the path integral is taken over the space-time configurations of the polarization field $P(\vec{x}, \tau)$,

$$Z = \sum_{\{P(x, \tau)\}} \exp \left[-\frac{S_E[P]}{\hbar} \right], \quad (11)$$

where

$$S_E[P] = \int_0^{\frac{\hbar}{k_B T}} d\tau d^3x \mathcal{L}_E[P] \quad (12)$$

and $\mathcal{L}_E[P]$ is the Lagrangian in Euclidean space-time. The action per unit time is now the Free energy F of the system (See Table I.). The salient point is that finite temperature imposes a *boundary condition in imaginary time* and the allowed configurations of the bosonic quantum fields are periodic in the imaginary time interval $\tau \in [0, \hbar\beta]$ ($\beta \equiv \frac{1}{k_B T}$) so that

$$\vec{P}(\vec{x}, \tau) = \vec{P}(\vec{x}, \tau + \hbar\beta). \quad (13)$$

The quantum fields are thus decomposed in terms of a discrete set of Fourier modes

$$P_n(\vec{x}, \tau) = \sum_{\vec{q}, n} P(\vec{q}, i\nu_n) e^{i(\vec{q} \cdot \vec{x} - \nu_n \tau)} \quad (14)$$

where

$$\nu_n = n \left(\frac{2\pi k_B T}{\hbar} \right) \quad (15)$$

are the discrete Matsubara frequencies; we recall that at $T = 0$ the (imaginary) frequency spectrum is a continuum. The response and correlation functions in (discrete) imaginary frequency

$$\chi_E(\vec{q}, i\nu_n) = \langle P(\vec{q}, i\nu_n) P(-\vec{q}, -i\nu_n) \rangle \quad (16)$$

can be analytically continued to yield the retarded response function

$$\chi_E(\vec{q}, i\nu_n) \rightarrow \chi_E(\vec{q}, \omega) = \chi_E(\vec{q}, z)|_{z=\omega+i\delta} \quad (17)$$

where ω is a real frequency; for writing convenience we will subsequently drop the “E” subscript in χ e.g. $\chi(\vec{q}, \omega) \equiv \chi_E(\vec{q}, \omega)$.

Like the parallel plates in the traditional Casimir effect, temperature removes modes of the field. In this case it is the frequencies not the wavevectors that assume a discrete character, namely

$$q = (\vec{q}, \omega) \rightarrow (\vec{q}, i\nu_n). \quad (18)$$

where ν_n are defined in (15). There are two key distinctions between the Casimir effects in space and in time to bear in mind:

- Temperature induces *periodic* boundary conditions, with discrete frequencies that include $n = 0$, whereas the corresponding $n = 0$ wavevectors are absent in the spatial case. Actually, the “missing” zero point energy associated with the $n = 0$ (frequency) mode does not depend on the boundary conditions, and so it does not effect the change in Casimir energy.
- In contrast to the noninteracting nature of the low-energy electromagnetic field, the modes at a typical quantum critical point are interacting. In the spatial Casimir effect, the finite correlation length is induced through the loss of the $n = 0$ mode. At an interacting quantum critical point, the discrete boundary conditions in imaginary time generate the thermal fluctuations in the fields in real time. These are fed back via interactions to generate a temperature-dependent gap in the spectrum and a finite correlation time. However complicated this feedback, provided the underlying system

is critical, temperature acting as a boundary condition in time will set the scale of the finite correlation time

$$\xi_\tau = \frac{\hbar}{\alpha k_B T}. \quad (19)$$

where $\alpha = O(1)$ is a constant of order unity. In cases where the quantum critical physics is universal, such as ferroelectrics in dimensions below $d = 3$, we expect the coefficient α to be also universal and independent of the underlying strength of the mode-mode coupling. Notice that ξ_τ is now related to the time-scale (1), which scales inversely with temperature (Fig. 1). The “temporal confinement” of the fields in imaginary time thus manifests itself as a finite response time in the real-time correlation and response functions.

For the quantum paraelectric at the zero temperature QFCP, the imaginary time correlation functions are scale-invariant

$$\chi(\vec{q}, i\nu) = \left. \langle P(\vec{q}, i\nu) P(-\vec{q}, -i\nu) \rangle \right|_{T=0} \sim \frac{1}{\nu^2 + c_s^2 q^2}. \quad (20)$$

At a finite temperature, we will see that this response function acquires a finite correlation time

$$\chi(\vec{q}, i\nu_n) \sim \frac{1}{\nu_n^2 + c_s^2 q^2 + \xi_\tau^{-2}}. \quad (21)$$

where

$$\xi_\tau^{-2} = 3\gamma \{ \langle P^2 \rangle_{T \neq 0} - \langle P^2 \rangle_{T=0} \}. \quad (22)$$

is determined by mode-mode interactions, where γ is the coupling constant describing the quartic interactions between the modes, to be defined in Sec IV. We note, as shall be shown explicitly in Section IV, that for dimensions d such that $1 < d < 3$, the feedback will be sufficiently strong such that ξ_τ will be *independent* of the coupling constant γ ; by contrast for $d > 3$ the feedback effects are weak so that there will be a γ -dependence of ξ_τ . The case $d = d_c^u = 3$ is marginal and will be discussed as a distinct case. At a temperature above a quantum critical point, the energy scale

$$\Delta(T) = \hbar \xi_\tau^{-1} = \alpha k_B T \quad (23)$$

will set the size of the gap in the phonon dispersion relation.

Reconnecting to our previous discussion, we remark that real-time response functions from expressions like (21) are obtained by analytic continuation to real frequencies $i\nu_n \rightarrow \omega$.

Since $\xi_\tau \sim \frac{1}{T}$, the dielectric susceptibility in the approach to the QFCP has the temperature-dependence

$$\chi(T) = \left. \chi(q, i\nu_n) \right|_{q=0, n=0} \sim \xi_\tau^2 \propto \frac{1}{T^2} \quad (24)$$

in contrast to the Curie form ($\chi \sim \frac{1}{T}$) associated with a classical paraelectric; this $1/T^2$ temperature-dependence was previously derived from a diagrammatic resummation,^{22,23} from analysis of the quantum spherical model²⁴ and from a renormalization-group study²⁵. As an aside, we note that the order of limits in (24) is not important because the polarization is not a conserved quantity. We note that this $1/T^2$ behavior in the dielectric susceptibility of the quantum paraelectric (in contrast to its Curie classical analog) has been observed experimentally^{16,40}.

Table I. summarizes the effects of spatial and temporal boundary conditions in the cases of the Casimir effect and finite-temperature at a quantum critical point respectively. This analogy emerges in an alternative determination of the coefficient \mathcal{C} in the Casimir energy (7) to be presented shortly. The traditional calculation of \mathcal{C} is performed using a regularization procedure with multiple cutoffs enforced by a zeta function^{1,34,35,36}. However, it is instructive to recompute the summations in the zero point energy using a Matsubara formalism³³, and this approach naturally brings out the analogy with finite temperature physics.

Suppose we reinterpret the discrete spatial frequency q_{zn} , as a ‘‘Matsubara frequency’’, identifying $cq_{zn} \equiv \nu_n$, then

$$cq_{zn} = nc \frac{\pi}{a} \equiv n \left(\frac{2\pi k_B T_C}{\hbar} \right) \quad (25)$$

where the effective Casimir temperature is given by

$$k_B T_C = \frac{\hbar c}{2a}, \quad (26)$$

so that $\beta_C = \frac{1}{k_B T_C} \equiv \frac{2a}{\hbar c}$, where we note that the ‘‘effective Casimir temperature’’ $T_C \sim \frac{1}{2a}$ (scales inversely with the interplane separation). We start by rewriting the zero point energy per unit area in (6) as

$$\frac{E_C}{A} = \frac{\hbar c}{2} \int \frac{d^2 q_\perp}{(2\pi)^2} \sum_{n \neq 0} \sqrt{q_\perp^2 + q_{zn}^2} = \frac{\hbar c}{2} \int \frac{d^2 q_\perp}{(2\pi)^2} \left(-q_\perp + \sum_n \sqrt{q_\perp^2 + q_{zn}^2} \right) \quad (27)$$

where the $-q_\perp$ term is introduced to remove the $n = 0$ term included in the sum. Notice how this term does not depend on the size of a . Now we are only interested in the *change* in the zero point energy as a result of the plates. In the limit of infinite plate separation

($a \rightarrow \infty$) the discrete interval in q_{zn} , $\Delta q_{zn} = \pi/a$, becomes infinitesimal; the summation over n in (6) can be replaced by an integral $\sum_n = \sum_n \frac{\Delta q}{\pi/a} = \frac{a}{\pi} \int dq_z$. Therefore the change in the zero point energy per unit area due to the presence of the plates is given by

$$\begin{aligned} \frac{\Delta E_C}{A} &= \frac{E_C}{A} - \frac{E_C}{A} \Big|_{a \rightarrow \infty} = \frac{\hbar c}{2} \int \frac{d^2 q_\perp}{(2\pi)^2} I(q_\perp, a), \\ I(q_\perp, a) &= \sum_{q_z = q_{zn}} \sqrt{q_\perp^2 + q_z^2} - a \int \frac{dq_z}{\pi} \sqrt{q_\perp^2 + q_z^2}. \end{aligned} \quad (28)$$

Notice that the subtracted $n = 0$ mode is not present in the difference in zero-point energies; this is because this mode is insensitive to the wavevector discretization. This fact was first noticed by Schwinger, who computed the Casimir effect with periodic boundary conditions and found that the inclusion of the $n = 0$ mode did not affect the final answer.⁴¹

Using the Matsubara method, we can now rewrite the sum in (28) as

$$c \sum_n \sqrt{q_\perp^2 + q_{zn}^2} = \sum_n F(i\nu_n); \quad \nu_n \equiv \frac{nc\pi}{a}, \quad (29)$$

where $F(z) = \sqrt{c^2 q_\perp^2 - z^2}$. The sum is now rewritten as a contour integral³³ around the poles at $z = i\nu_n$ of the Bose function $n(z) = \frac{1}{e^{\hbar\beta z} - 1}$

$$\sum_n F(i\nu_n) = \frac{\hbar}{k_B T} \int_C \frac{dz}{2\pi i} F(z) \left(n(z) + \frac{1}{2} \right). \quad (30)$$

The integral in (30) can be evaluated by distorting the contour around the branch cuts in $F(z)$ that extend from $z = \pm cq_\perp$ to infinity, to obtain

$$I(q_\perp, a) = \frac{\hbar\beta_C}{c} \int_C \frac{dz}{2\pi i} \sqrt{c^2 q_\perp^2 - z^2} \left(n(z) + \frac{1}{2} \right) - \{\beta_C \rightarrow \infty\}, \quad (31)$$

where we use the relation $\beta_C \sim a \rightarrow \infty$ in the second term of $I(q_\perp, a)$. When we distort the contour around each of these two branch cuts, we obtain

$$\begin{aligned} I(q_\perp, a) &= -2 \frac{\hbar\beta_C}{c} \int_{cq_\perp}^{\infty} \frac{d\omega}{\pi} \sqrt{\omega^2 - c^2 q_\perp^2} \left(n(\omega) + \frac{1}{2} \right) - \{\beta_C \rightarrow \infty\} \\ &= -2 \frac{\hbar\beta_C}{c} \int_{cq_\perp}^{\infty} \frac{d\omega}{\pi} \sqrt{\omega^2 - c^2 q_\perp^2} n(\omega), \end{aligned} \quad (32)$$

where the factor of two is due to the number of branch cuts. The change in zero point energy is then given by

$$\frac{\Delta E_C}{A} = -2\hbar^2 \beta_C \int_{\omega > q_\perp} \frac{d^2 q_\perp d\omega}{(2\pi)^3} n(\omega) \sqrt{\omega^2 - c^2 q_\perp^2}. \quad (33)$$

Carrying out the integral over q_\perp , we obtain

$$\frac{\Delta E_C}{A} = -\frac{\hbar^2 \beta_C}{6\pi^2 c^2} \int d\omega \omega^3 n(\omega). \quad (34)$$

Changing variables to $x = \frac{\hbar\omega}{k_B T}$ in (34), we find it is formally identical to the thermal free energy F of black-body radiation^{42,43} in a volume $V = aA$ at a finite temperature $\beta_C^{-1} = k_B T_C = \frac{\hbar c}{2a}$ where

$$\frac{F}{A} = -a \frac{(k_B T_C)^4}{3\pi^2 c^3 \hbar^3} \int dx x^3 n(x) = \frac{\Delta E_C}{A}. \quad (35)$$

Traditionally, we think of black body radiation as the consequence of an excitation of thermal modes. Yet a finite temperature generates an entropy $S = -\frac{dF}{dT}$, so that temperature results in a reduction of the free energy. Our simple calculation shows that both the Casimir effect and black-body radiation share a common space-time origin: both are consequences of boundary conditions, resulting in the *removal* of zero-point fluctuation modes from the vacuum.

Rescaling the integral (34) and replacing $\beta_C = \frac{2a}{\hbar c}$, we obtain

$$\frac{\Delta E_C}{A} = -\frac{1}{6\pi^2 \hbar^2 \beta_C^3 c^2} \overbrace{\int dx \frac{x^3}{e^x - 1}}^{\frac{\pi^4}{15}} = -\frac{\pi^2}{720} \frac{\hbar c}{a^3} \quad (36)$$

in agreement with the traditional derivations^{1,34,35,36}; we note that in our treatment we did not have to introduce cutoffs since we calculated the sum directly. Because the Casimir energy density (36) is proportional to \hbar and to a^{-3} , it is numerically a very small effect and can only be observed on micrometer length-scales^{29,30,31,32}. By contrast Casimir energy per unit volume ($\frac{E}{V} \sim \frac{1}{a^4}$) means that the analogous free energy density (see Table I.) associated with the boundary condition in imaginary time is proportional to T^4 . Furthermore we recover the Debye specific heat form, $c_v \sim T^3$, that results from the interplay between gapless lattice modes and external constraints imposed by temperature.

III. FINITE-SIZE SCALING IN TIME

The spatial and temporal Casimir phenomena just described result from the effects of boundary conditions on scale-free quantum fluctuations. A system at a quantum critical point is gapless and has fluctuations on all length- and time-scales, and it is exactly for this

reason that it is sensitive to spatial and temporal constraints. This phenomenon has been well studied in the context of classical critical points, where order parameter fluctuations occur at all length-scales³. These methods can be extended to understand the influence of temperature at a quantum critical point as a finite-size scaling effect in imaginary time (or imaginary frequency).

At classical criticality, the wavevector-dependent susceptibility is scale-invariant of the form

$$\chi(q, t = 0) = \frac{\chi_0}{q^{2-\eta}} \quad (37)$$

where t is the reduced temperature ($t = |T-T_c|$) and η is one of several exponents that characterizes the critical point. For $t \neq 0$, the correlation length ξ is finite and we have

$$\chi(q, t) = \frac{1}{q^{2-\eta}} \Phi(q\xi) \quad (38)$$

where the scaling function $\Phi(x)$ is universal and is determined by the nature of the critical point³. Let us now impose a fixed boundary condition (finite L) as depicted schematically in Figure 2a. In this case, our wavevector-dependent susceptibility takes the form

$$\chi(q, t, L) = \frac{1}{q^{2-\eta}} \Phi_0(q\xi, qL) = \frac{1}{q^{2-\eta}} \tilde{\Phi}_0(qL, \frac{L}{\xi}) \quad (39)$$

where $\xi = \xi(t)$ and $\tilde{\Phi}_0(x, y) = \Phi_0(x/y, x)$.

In the case where $L \ll \xi$ (see Figure 2a), L plays the role of an effective correlation length and the q -dependent susceptibility can be written as

$$\chi(q, L) = \frac{1}{q^{2-\eta}} \tilde{\Phi}_0(qL, 0) \quad (40)$$

where $\chi(q, L)$ is no longer t -dependent. The limit $q \rightarrow 0$ describes the physics on length-scales $\Delta x \sim 1/q \gg L$ much longer than L ; by contrast, the limit $q \rightarrow \infty$ describes the physics on length-scales $\Delta x \sim 1/q \ll L$. At small q , all dependence on q must vanish, so $\tilde{\Phi}_0(qL, 0) \sim (qL)^{2-\eta}$ in this limit; it then follows that the uniform susceptibility of a classical critical system inside a slab of dimension L (where $L \ll \xi$) is given by

$$\chi(q = 0, L) \sim L^{2-\eta}. \quad (41)$$

Returning to the response and correlation functions in (16) and (21), let us now see how this works at a quantum critical point. The finite-temperature susceptibility obtained in

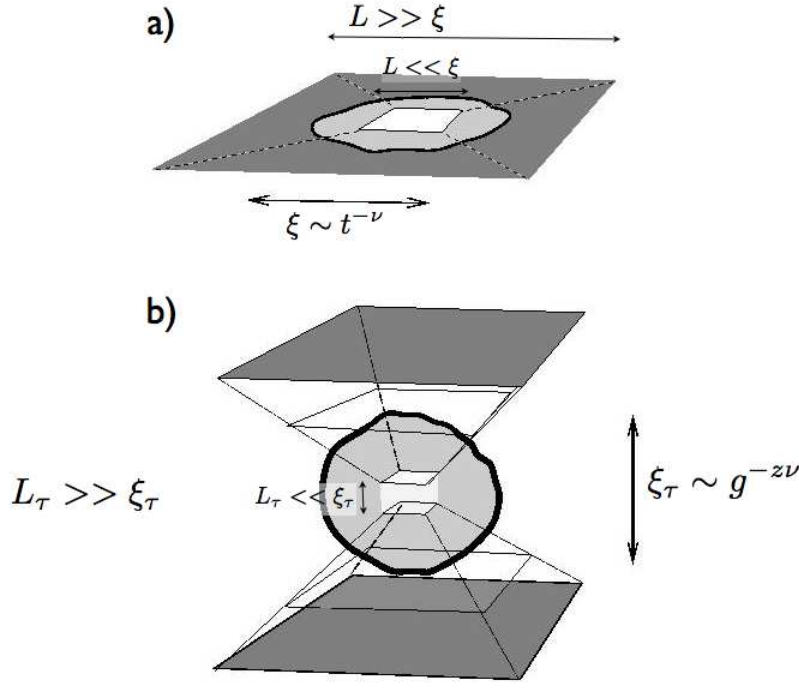


Figure 2: Schematic of finite-size effects (a) at a classical and at a (b) quantum critical point where the appropriate lengths are defined in the text.

(21) can be analytically continued into the complex plane. Along the imaginary axis the uniform susceptibility takes the form

$$\chi(q = 0, i\nu, T) = \chi(i\nu, T) = \frac{1}{\nu^2} \tilde{\Phi}_1(\nu L_\tau, \frac{L_\tau}{\xi_\tau}) \quad (42)$$

where $L_\tau = \frac{\hbar}{k_B T}$ is finite time determined by temperature (see Fig. 1), ξ_τ is the correlation time set by the tuning parameter (g) as discussed below in the text and where, as before, $i\nu$ is the analytic continuation of the (real) frequency ω onto the complex axis. When $L_\tau << \xi_\tau$ (see Figure 2b), time fluctuations become truncated by the finite time dimension, and L_τ becomes an *effective correlation time*. With the scaling function $\tilde{\Phi}_1 = \tilde{\Phi}_1(\nu L_\tau, 0)$, the frequency-dependent susceptibility (see (21)), then takes on a scaling form

$$\tilde{\Phi}_1(x) = \frac{x^2}{1 + x^2}. \quad (43)$$

Since this system cannot probe time-scales longer than L_τ , we must have $\lim_{x \rightarrow 0} \Phi_1(x) \rightarrow x^2$; it then follows that the static uniform susceptibility has the form

$$\lim_{x \rightarrow 0} \chi(i\nu) = \frac{1}{\nu^2} x^2 = L_\tau^2 \propto \frac{1}{T^2} \quad (44)$$

so that we have a familiar result^{22,23,24,25}.

The quantum paraelectric is a particularly simple example of the boundary effects of temperature, since here the dynamical exponent $z = 1$ and $\eta = 0$. In the more general case, momentum and frequency will enter with different powers where $[q^z] = [\nu]$. At the quantum critical point, since $\chi(q) \sim \frac{1}{q^{2-\eta}}$, it follows that $\chi(\nu) \sim \frac{1}{\nu^{(2-\eta)/z}}$; the general scaling form for the frequency-dependent susceptibility becomes

$$\chi(i\nu, T) = \frac{1}{\nu^{(2-\eta)/z}} \Phi_2(\nu L_\tau) \quad (45)$$

so that the static susceptibility is given by

$$\chi(0, T) \propto \frac{1}{T^{(2-\eta)/z}} \quad (46)$$

in the vicinity of a QCP. Just as a classical critical point has influence on the thermodynamic properties of a system that is not infinite in spatial extent, its quantum counterpart affects responses at finite temperature. In a nutshell, finite-size effects explain why quantum criticality, strictly a $T = 0$ phenomenon, has impact on real experiment performed at nonzero temperatures.

Another way to introduce finite-size effects is to impose boundaries on a system that is tuned to its critical point. Temperature is the tuning parameter near a classical critical point; in the absence of spatial constraints, critical fluctuations occur on all length-scales and the correlation length (ξ) and the susceptibility (χ) diverge with exponents $\xi \sim t^{-\tilde{\nu}}$ and $\chi \sim t^{-\gamma}$ respectively where $t = |\frac{T-T_c}{T_c}|$ is the reduced temperature. Here we introduce the critical exponent $\tilde{\nu}$, because ν is already in use as a frequency. If we tune the system to a given value of t and correlation length ξ and then confine it in a box of size L , (see Fig. 2a), then we write³

$$\chi = t^{-\gamma} \Phi_3\left(\frac{L}{\xi}\right) \quad (47)$$

which translates into

$$\chi = t^{-\gamma} \bar{\Phi}_3\left(\frac{L}{t^{-\tilde{\nu}}}\right) \quad (48)$$

where $\Phi_3(x)$ and $\bar{\Phi}_3(x)$ are scaling functions. In the limit $x \rightarrow 0$, we expect the susceptibility in (48) to be just a function of L , namely $\chi = \chi(L)$; this also means that it should not have any t -dependence. Assuming that $\bar{\Phi}_3(x) \sim x^p$, we then find that

$$\chi \sim t^{-\gamma} \left(\frac{L}{t^{-\tilde{\nu}}}\right)^p \sim t^{-\gamma} \left(\frac{L}{t^{-\tilde{\nu}}}\right)^{\frac{\gamma}{\tilde{\nu}}} \sim L^{\frac{\gamma}{\tilde{\nu}}} \quad (49)$$

so that χ is now a power-law function of the box size. We note that comparison of the two expressions for $\chi(L)$, (41) and (49), yield the scaling relation

$$(2 - \eta)\tilde{\nu} = \gamma \quad (50)$$

which results from the fact that these critical exponents are not independent³. The behavior of other thermodynamic functions for finite L can be found in a similar fashion³. The key idea here is that a classical critical point influences the properties of a spatially restricted system in its vicinity, even though it does not have critical fluctuations on all length-scales.

Similar reasoning can be used when a system is tuned into a quantum critical point; for a quantum paraelectric, the tuning parameter g is the reduced pressure $g = |\frac{P-P_c}{P_c}|$. Introducing a fixed L_τ (see Fig. 2b) (associated with a finite temperature), we can write

$$\chi = g^{-\gamma} \Phi_4 \left(\frac{L_\tau}{\xi_\tau} \right) \quad (51)$$

in complete analogy with the classical finite-size case described above. Now we must develop a relation between ξ_τ and the tuning parameter g ; the analogous situation ($\xi \sim t^{-\tilde{\nu}}$) is more straightforward in the classical case. From the form of the scaling function in (42), we see that dimensionally

$$[\xi_\tau] = [L_\tau] = \left[\frac{1}{T} \right] \quad (52)$$

are equivalent when $\hbar = k_B = 1$. The dispersion relation $\omega = cq^z$ yields $[\xi_\tau] = [\xi^z]$; this combined with $\xi \sim g^{-\tilde{\nu}}$ and (52) results in the dimensional equivalences

$$[g] = [\xi^{-\frac{1}{\tilde{\nu}}}] = [\xi_\tau^{-\frac{1}{z\tilde{\nu}}}] = [L_\tau^{-\frac{1}{z\tilde{\nu}}}] = [T^{\frac{1}{z\tilde{\nu}}}] \quad (53)$$

(51) and (53) together therefore yield

$$\chi = g^{-\gamma} \bar{\Phi}_4 \left(\frac{L_\tau}{g^{-z\tilde{\nu}}} \right) \quad (54)$$

which is reminiscent of (48). Here $\bar{\Phi}_4(x)$ is a crossover function; when $x \rightarrow 0$, we expect $\chi = \chi(L_\tau)$, whereas we should recover the zero-temperature result ($\chi \sim g^{-\gamma}$) when $x \rightarrow \infty$. Then we get

$$\chi \sim g^{-\gamma} \left(\frac{L_\tau}{g^{-z\tilde{\nu}}} \right)^{\frac{\gamma}{z\tilde{\nu}}} \sim L_\tau^{\frac{\gamma}{z\tilde{\nu}}} \sim T^{-\frac{\gamma}{z\tilde{\nu}}} \quad (55)$$

and the temperature-dependence emerges naturally from finite-size arguments. Therefore a (zero-temperature) quantum critical point can influence thermodynamic properties of a

Classical to Quantum Scaling

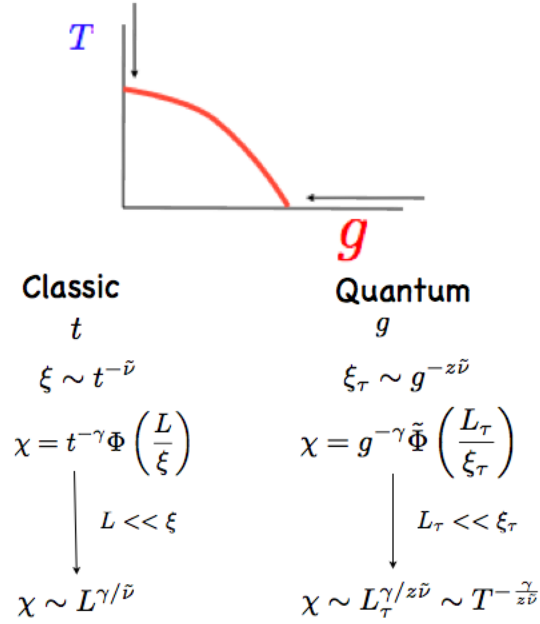


Figure 3: Overview of the finite-size scaling at classical and quantum critical points; here $\tilde{\nu}$ is the exponent associated with the spatial correlation length since ν has already been used in the text as a frequency.

system at finite temperatures just as a finite-size system displays aspects of classical critical phenomena despite its spatial constraints. A comparison of (46) and (55) indicates that the scaling relation (50) holds in the vicinity of a quantum critical point since the dynamical exponent z appears in both expressions and thus cancels out. A schematic overview of the finite-size scaling arguments we have presented here is displayed in Figure 3.

Naturally this finite-size scaling approach can also yield the temperature-dependences of the specific heat and the polarization of a quantum critical paraelectric. Following our previous discussion, we expect its free energy at finite temperature to take the form

$$f_{qm}(g, L_\tau) = g^{2-\alpha} \Phi_5\left(\frac{L_\tau}{\xi_\tau}\right) = g^{2-\alpha} \tilde{\Phi}_5\left(\frac{L_\tau}{g^{-z\tilde{\nu}}}\right) \quad (56)$$

where we have used the dimensional analysis in (53). For $L_\tau \ll \xi_\tau$, we expect $f_{qm} = f_{qm}(L_\tau)$ so that

$$f_{qm}(L_\tau) \sim g^{2-\alpha} \left(\frac{L_\tau}{g^{-z\tilde{\nu}}}\right)^{-\frac{(2-\alpha)}{z\tilde{\nu}}} \sim L_\tau^{-\frac{2-\alpha}{z\tilde{\nu}}} \sim T^{\frac{2-\alpha}{z\tilde{\nu}}} \quad (57)$$

and the temperature-dependent specific heat is

$$c_V = T \partial^2 f_{qm} / \partial T^2 \sim T^{\frac{2-\alpha}{z\nu}-1} \quad (58)$$

in the vicinity of a quantum critical point. Similarly the temperature-dependence of the polarization is

$$P \sim g^\beta \bar{\Phi}_5 \left(\frac{L_\tau}{\xi_\tau} \right) \sim T^{\frac{\beta}{z\nu}} \quad (59)$$

and we note that $P(E) = \partial f_{qm} / \partial E|_{g=0} \sim E^{1/\delta}$ is temperature-independent, since finite-temperature scaling does not affect field-behavior.

Before we turn to the specific exponents associated with the quantum paraelectric, let us summarize the mapping between classical and quantum scaling; please see Figure 3. We have found that the T - and g -dependent exponents at a quantum critical point (QCP) are distinct but related, as expected from a finite-size scaling approach. Here the effective dimensionality is $D = d + z$ where d is the spatial dimension and z is the dynamic exponent defined by the dispersion $\omega = cq^z$. Simple scaling relations at classical and quantum criticality are summarized in Figure 3. The key notion is that at a quantum critical point, finite-temperature effects correspond to the limit $L_\tau \ll \xi_\tau$; in this case L_τ becomes the effective correlation length in time, and the temperature-dependences follow. We note that we expect this finite-size approach to work for dimensions $d < d_c^u$ where there will be logarithmic corrections to scaling in the upper critical dimension d_c^u .

Now let us now be more specific with exponents for the quantum paraelectric case. At criticality the temperature-dependence of the paraelectric susceptibility (χ) can be found by a soft-mode analysis^{9,44} where the Lagrangian, referred to in (12) and introduced more specifically in Section IV, is treated as a self-consistent Gaussian theory. The critical exponents for the quantum paraelectric are therefore those of the quantum spherical model.²⁴ For the case of interest ($D = d + z = 3 + 1 = 4$), the quantum spherical model has exponents $\tilde{\nu} = 1/(D - 2) = 1/2$ and $\gamma = 2/(D - 2) = 1$, so that $\gamma_{th} = \frac{\gamma}{z\tilde{\nu}} = 2$ and we recover the $\chi^{-1} \sim T^2$ scaling found earlier in (24) and (44). Similarly, using (58) and the spherical exponents ($\alpha = \frac{D-4}{D-2} = 0$ here) to obtain $c_v \sim T^3$. Application of dimensional analysis in (53) to the specific case of the $d = 3$ quantum paraelectric results in

$$[g] = [T^2] \quad \rightarrow g \sim T^2 \quad (60)$$

which yields a quadratic dependence of the scaling variable g on temperature; this relation was experimentally observed^{15,45} in *STO* where g is the pressure difference or oxygen concentration.

Finally we note that the finite-temperature scaling that we have discussed suggests a particular scaling form for the uniform dynamical susceptibility. If we take the scaling expression (45) for $\chi(i\nu, T)$, and analytically continue it to the real frequency axis ($i\nu \rightarrow \omega$) then we obtain

$$\chi(\omega, T) = \frac{1}{\omega^2} \tilde{\Phi}_2(\omega L_\tau) \quad (61)$$

for the uniform dynamical susceptibility. Recalling from (19) that L_τ scales inverses with temperature, we conclude that this uniform susceptibility satisfies the “ $\frac{\omega}{T}$ ” scaling form

$$\chi(\omega, T) = \frac{1}{\omega^2} F\left(\frac{\omega}{T}\right) \quad (62)$$

that is similar to that observed in other systems at quantum criticality^{46,47}. The predictions for experiment are summarized in Table II. We note that since we are in the upper critical dimension, there will be logarithmic corrections to this scaling but we do not expect these to be experimentally important for the temperature dependences described here; however they will be considered later in the paper (Section VI)

Table II. Observables for a $D = 4$ QPE in the Vicinity of a QFCP

Observable	T-Dependences ($g=0$)	g-Dependences ($T=0$)
Specific Heat	$c_v \sim T^3$	$c_v \sim g^0$
Polarization	$P \sim T^1$	$P \sim g^{\frac{1}{2}}$
Susceptibility	$\chi \sim T^{-2}$	$\chi \sim g^{-1}$

$$\begin{aligned} P &\sim E^{\frac{1}{3}} \\ \chi(\omega, T) &= \frac{1}{\omega^2} F\left(\frac{\omega}{T}\right) \end{aligned}$$

IV. SELF-CONSISTENT MEAN-FIELD THEORY

A. Soft-Mode Analysis and Gap Equation

In this section we apply self-consistent mean-field theory to recover temperature-dependences of the quantum paraelectric previously found via finite-size scaling; we also

study the crossover behavior between the classical and the quantum critical points, and in the process determine the temperature-pressure phase diagram. This will then give us the opportunity to make further comparison with experiment.

The Lagrangian in Euclidean space-time, \mathcal{L}_E in (12), for displacive ferroelectrics is

$$\mathcal{L}_E = \frac{m}{2} [(\partial_\tau P)^2 + c^2(\nabla P)^2 + rP^2] + \frac{\gamma}{4}P^4, \quad (63)$$

where $P(x, t)$ is the order parameter, a polarization field normalized by the the charge density that has dimensions of length; c is the velocity of the compression sound mode associated with the soft mode and r is the tuning coupling parameter such that $g = r - r_c$. This is, in essence, a time-dependent Landau-Ginzburg theory that describes the long-wavelength, low frequency physics in the vicinity of the ferroelectric quantum critical point. The first term in the Lagrangian is the kinetic energy responsible for dynamics. The parameter r tunes the system through the critical point (e.g. pressure, doping or temperature) where its value is $r = r_c$ (which corresponds to $g = 0$). The quantity

$$\Omega_0^2 \equiv r - r_c = g, \quad (64)$$

defines a bare phonon frequency Ω_0 . Here γ is a material constant that determines the strength of the nonlinear couplings between the normal modes.

For our development, we shall absorb m , c , \hbar and k_B into a rescaling of P through a redefinition of parameters

$$\sqrt{m}P = \tilde{P}, \quad \frac{x}{c} = \tilde{x}, \quad \frac{\gamma}{m} = \tilde{\gamma}, \quad \frac{\hbar}{k_B T} = \frac{1}{\tilde{T}} = \beta \quad (65)$$

where we have effectively set $m = c = \hbar = k_B = 1$. For convenience we drop the tildas and the Lagrangian becomes

$$\mathcal{L}_E \rightarrow \frac{1}{2} [(\partial_\tau P)^2 + (\nabla P)^2 + rP^2] + \frac{\gamma}{4}P^4, \quad (66)$$

which is now recognizable as that associated with the ϕ^4 model. The quantum partition function describing the quantum critical behavior is determined by the path integral

$$Z = \int \mathcal{D}[P] e^{-S[P]}, \quad (67)$$

where

$$S[P] = \int_0^\beta d\tau \int d^d x \mathcal{L}_E[P] \quad (68)$$

is the action and the measure \mathcal{D} indicates an integration over all space-time configurations of the polarization field. Although our principle interest lies in three-dimensional ferroelectrics, for generality of discussion, we have introduced d spatial dimensions. This is nothing more than the partition function of a $D = d + 1$ dimensional classical problem, with a finite periodic boundary condition in the imaginary time direction.

We now revisit the classic soft-mode analysis of a quantum critical ferroelectric. The temperature-dependent paraelectric susceptibility and soft-mode spectrum can be found by a soft-mode analysis^{9,44}, where (66) is approximated as a self-consistent Gaussian theory where interaction feedback is considered via its renormalization of quadratic terms. This procedure is equivalent to the replacement

$$P^4 \rightarrow 6P^2\langle P^2 \rangle, \quad \frac{\gamma}{4}P^4 \rightarrow \frac{3\gamma}{2}\langle P^2 \rangle P^2 = \frac{1}{2}\Sigma P^2 \quad (69)$$

where

$$\Sigma = 3\gamma\langle P^2 \rangle \quad (70)$$

is the Hartree self-energy that provides a mean-field treatment of the feedback effects of mode-mode coupling.

In the 1950's, physicists discovered that these kinds of mode-mode couplings were not sufficient to understand the detailed scaling properties of classical critical phenomena and the appearance of anomalous critical exponents below four dimensions. However, we will stick with the self-consistent Gaussian approximation, which provides many of the sentient aspects of the physics without using the detailed heavy machinery of the renormalization group. With the foresight of modern critical phenomenon, we now know that the mode-mode coupling theory is exact for the “spherical model” generalization of ϕ^4 theory in which the order parameter has N components and N is taken to infinity. In this theory the Hartree self-energy has the form

$$\Sigma_N = 3\gamma_N \left(\frac{\langle P^2 \rangle}{N} \right) \quad (71)$$

where γ_N is weakly dependent on N . Here we have interpolated the large N result (71) to the case relevant for uniaxial ferroelectrics ($N = 1$), and this procedure yields (70); we expect that temperature-dependences are robust to this procedure, though specific coefficients are not. The procedure described in (69) are equivalent to replacing \mathcal{L}_E by the Gaussian Lagrangian

$$\mathcal{L}_G = \frac{1}{2}P \left[-\partial_\tau^2 - \nabla^2 + r + \Sigma \right] P \quad (72)$$

subject to the additional consistency requirement (70).

The Gaussian approximation to the partition function is then given by

$$Z_G = \int d[P] e^{-S_G[P]}, \quad (73)$$

where

$$S_G = \int_0^\beta d\tau \int d^d x \mathcal{L}_G[P]. \quad (74)$$

The quantity $e^{-S_G[P]}$ is the Gaussian weight associated with the configuration $\{P\}$. We can regard the function $P_x \equiv P(\vec{x}, \tau) \equiv \langle \vec{x}, \tau | P \rangle$ as the components P_x of an infinite dimensional vector $|P\rangle = \int d^d x d\tau |\vec{x}, \tau\rangle P(\vec{x}, \tau)$. From this perspective, the partition function Z_G is just a Gaussian integral over the “components” $P_{\vec{x}, \tau}$ of the configuration vector $|P\rangle$, acted on by the matrix $-G^{-1} = -G_0^{-1} + \Sigma$. The action can be written in the short-hand

$$S_G = \int_{x', x} P_{x'} [-G_0^{-1} + \Sigma]_{x', x} P_x, \quad (75)$$

where $P_x \equiv P(\vec{x}, \tau)$ and $\int_x \equiv \int d^d x d\tau$.

In spacetime, the “matrix” G_0^{-1} is represented by the operator

$$[G_0^{-1}]_{x', x} = \delta^{(d)}(\vec{x}' - \vec{x}) \delta(\tau' - \tau) [-\partial_\tau^2 - \nabla^2 + r] \quad (76)$$

and

$$-G_{x', x}^{-1} \equiv [-G_0^{-1} + \Sigma]_{x, x'} = \delta^{(d)}(\vec{x}' - \vec{x}) \delta(\tau' - \tau) [-\partial_\tau^2 - \nabla^2 + r + \Sigma]. \quad (77)$$

The relationship $G^{-1} = G_0^{-1} - \Sigma$ is an alternative version of the Dyson equation $G = G_0 + G_0 \Sigma G$ and can be represented by the Feynman diagrams shown in Fig. 4 (a). In a discrete Gaussian integral over the vector S_i , with weight factor $e^{-\frac{1}{2} S_i M_{ij} S_j}$, the inverse matrix M_{ij}^{-1} determines the variance of the fluctuations of S_i , $\langle S_i S_j \rangle = [M^{-1}]_{ij}$. Similarly, $-G_{x', x}^{-1} \equiv M_{x', x}$ is a matrix with a continuous basis labelled by the positions in spacetime $x \equiv (\vec{x}, \tau)$, whose inverse $M_{x, x'}^{-1} = -G_{x, x'}$ determines the (time-ordered) fluctuations of the polarization field:

$$\langle T P(x) P(x') \rangle = -\langle x | G | x' \rangle = -G(x - x') \quad (78)$$

The magic in this relation, is that by introducing the time-ordering operator T , we are able to relate the statistical average of $P(\vec{x}, \tau)$ inside the path integral to the time-ordered Green’s function of the Heisenberg operators $\hat{P}(\vec{x}, \tau)$. In this way, we identify G as the

Greens function of the polarization field, while G_0 is the bare Green's function of the non-interacting problem with $\gamma = 0$.

The above relationships become more transparent when we diagonalize the action S_G by recasting the polarization in terms of their Fourier components, writing

$$P(\vec{x}, \tau) = \frac{1}{\sqrt{\beta V}} \sum_{\vec{q}, i\nu_n} P(\vec{q}, i\nu_n) e^{i\vec{q} \cdot \vec{x} - i\nu_n \tau}, \quad (79)$$

where (βV) is the volume of space-time. In the momentum-frequency basis, the components of $|P\rangle$, $P(\vec{q}, i\nu_n) \equiv \langle \vec{q}, i\nu_n | P \rangle$ form a discrete vector. The action takes the form

$$S_G = - \sum_{q=(\vec{q}, i\nu_n)} P(q) G^{-1}(q) P(-q). \quad (80)$$

If we Fourier transform the derivative terms inside the Green's function (78), replacing $\partial_\tau \rightarrow -i\nu_n$ and $\vec{\nabla} \rightarrow i\vec{q}$ we see that the resulting Green's function is now diagonal:

$$G(q) \equiv G(\vec{q}, i\nu_n) = [(i\nu_n)^2 - q^2 - r - \Sigma]^{-1}, \quad (81)$$

so the action is diagonalized in this basis. The poles of $G(\vec{q}, \omega)$ determine the dispersion relation ω_q for the dispersive polarization modes

$$\omega_q^2 = q^2 + \Delta^2 \quad (82)$$

where here we have introduced the gap function

$$\Delta(r, T)^2 = r + \Sigma(r, T). \quad (83)$$

This quantity vanishes at both quantum and classical critical points where there are scale-free (gapless) fluctuations. At the quantum critical point where $T_c = 0$, $\Delta(r_c, 0) = r_c + \Sigma(r_c, T = 0)$, so that we can eliminate $r_c = -\Sigma(r_c, T = 0)$, to obtain

$$\Delta(r, T)^2 = \Omega_0^2 + [\Sigma(r, T) - \Sigma(r_c, 0)]. \quad (84)$$

where $\Omega_0^2 = (r - r_c) = g$.

From (78) and (79), the amplitude of the polarization fluctuations is given by

$$\langle P^2 \rangle = -G(0, 0) = \frac{1}{\beta V} \sum_q G(q) e^{iqx} |_{x=0}, \quad (85)$$

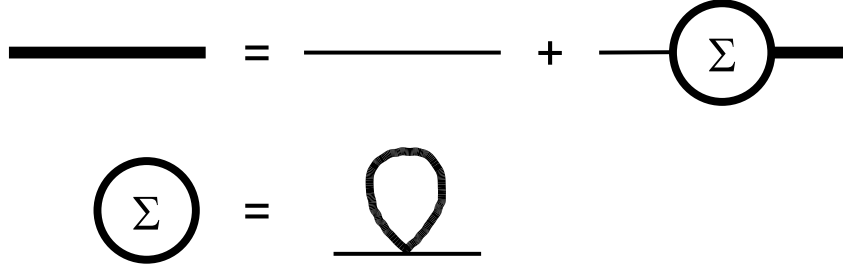


Figure 4: Diagrammatic Representation of (a) the Dyson Equation and (b) the Self-Consistent Hartree Self-Energy described in the text

so the self-consistency (70) condition $\Sigma = 3\gamma\langle P^2 \rangle$ can now be written

$$\Sigma(r, T) = (-3\gamma)T \sum_n \int \frac{d^3q}{(2\pi)^3} G(q, i\nu_n), \quad (86)$$

where $\Sigma(r, T)$ is the temperature-dependent self-energy. This expression can be understood as the self-consistent Hartree approximation to the phonon self energy, as shown in Fig. 4. By converting the discrete Matsubara summation to a contour integral, deformed around the poles $z = \pm\omega(q)$ in the dispersion relation, we can convert this expression to the form

$$\Sigma(r, T) = 3\gamma \int \frac{d^d q}{(2\pi)^d} \frac{[n(\omega_q) + \frac{1}{2}]}{\omega_q}. \quad (87)$$

At the quantum critical point ($r = r_c$ and $T = 0$), we have $\omega_q = q$ and $n(\omega_q) = 0$ so that

$$\Sigma(r_c, 0) = 3\gamma \int \frac{d^d q}{(2\pi)^d} \frac{1}{2q}, \quad (88)$$

and using (84), we can write the gap function as

$$\begin{aligned} \Delta^2 &= \Omega_0^2 + 3\gamma \int \frac{d^d q}{(2\pi)^d} \left(\frac{[n(\omega_q) + \frac{1}{2}]}{\omega_q} - \frac{1}{2q} \right), \\ \omega_q &= \sqrt{q^2 + \Delta^2}. \end{aligned} \quad (89)$$

B. Temperature-Dependence of the Gap at the Quantum Critical Point.

The temperature-dependence of the gap is of particular interest since it is crucial for calculating the dielectric susceptibility. In the paraelectric phases, we can use the temperature-

dependent gap to determine the dielectric susceptibility χ . Writing

$$\chi = \chi(q, \omega) \Big|_{\vec{q}, \omega=0} = \langle P(q)P(-q) \rangle \Big|_{q=0} = -G(\vec{q}, \omega) \Big|_{\vec{q}, \omega=0}, \quad (90)$$

we use (81) and (83) to express it as

$$\chi^{-1}(r, T) = \Delta^2(r, T). \quad (91)$$

At the quantum critical point $\Omega_0^2 = 0$, so the gap equation (89) becomes

$$\Delta^2(r_c, T) = 3\gamma \int_0^{q < q_{max}} \frac{d^d q}{(2\pi)^d} \left\{ \frac{(n(\omega_q) + \frac{1}{2})}{\omega_q} - \frac{1}{2q} \right\}. \quad (92)$$

We notice that both thermal and quantum fluctuations contribute to this expression.

Even though the mean field gap equation is only formally exact in the spherical mean-field limit, it is sufficient to illustrate the qualitative influence of temperature on the correlation length and gap at the quantum critical point. The upper cut-off of the above integral depends on q_{max}^{d-3} , and it can not be removed in dimensions $d > 3$. However, in dimensions $d < 3$, the integral is convergent in the ultraviolet and the upper cutoff in (92) can be entirely removed. Thus, for $d < 3$, the only scale in the problem is temperature itself. The integral is also convergent in the infrared provided $d > 1$. The spatial dimensions $d = 1$ and $d = 3$ correspond to spacetime dimensions $D = d + 1 = 2$ and $D = d + 1 = 4$, which are the well-known upper and lower critical dimensions of the ϕ^4 theory. This provides us with a dimensional window $1 < d < 3$ where inverse temperature acts as a cut-off in time. In this range, the temperature-dependence of the gap

$$\Delta(T) = \alpha_d T \quad (93)$$

is independent of the strength of the coupling constant γ and the cutoff, a feature that can be illustrated already within mode-coupling theory. Recalling that $\Delta(T) = \frac{1}{L_\tau}$ when $\hbar = k_B = 1$ (see (23)), we note that confirmation of (93) is consistent with our earlier discussion (see after (22)) that L_τ is independent of coupling constant; in this dimensional window, temperature is a boundary effect in (imaginary) time and is the only temporal scale in the problem.

In order to calculate α_d , we rewrite the gap equation at criticality as

$$\frac{\Delta^2}{T^2} = \alpha^2 = \frac{3\gamma}{T^2} \Gamma_d \int_0^\infty \frac{q^{d-1} dq}{(2\pi)^d} \left\{ \frac{(n(\omega_q) + \frac{1}{2})}{\omega_q} - \frac{1}{2q} \right\}, \quad (94)$$

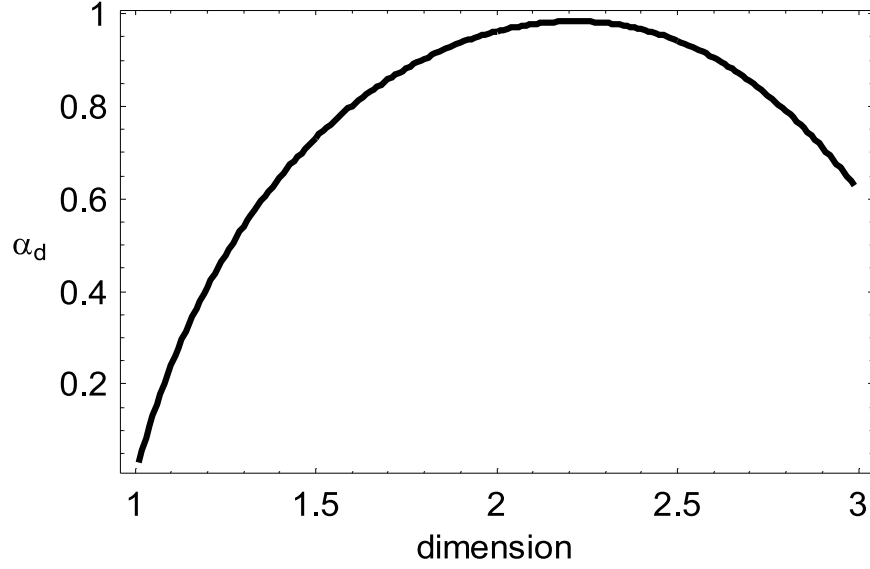


Figure 5: Dependence of $\alpha_d(T \rightarrow 0)$ on dimensionality.

where $\Gamma_d q^{d-1} dq$ ($\Gamma_d = \frac{2\pi^{d/2}}{\Gamma(d/2)}$) is the d-dimensional volume measure. Rescaling $\Delta = \alpha_d T$ and $q = uT$, we obtain

$$F_d[\alpha] = T^{3-d} \alpha_d^2 / \gamma \quad (95)$$

where

$$F_d[\alpha] = \frac{3}{(2\sqrt{\pi})^d \Gamma(d/2)} \int_0^\infty u^{d-1} du \left\{ \frac{\coth(\frac{1}{2}\sqrt{u^2 + \alpha^2})}{\sqrt{u^2 + \alpha^2}} - \frac{1}{u} \right\}. \quad (96)$$

For $d < 3$, the temperature prefactor on the right-hand side of (95) vanishes $T \rightarrow 0$, so a consistent solution requires α_d to satisfy

$$F_d[\alpha_d] = 0. \quad (97)$$

At a small finite temperature, we can expand around $\alpha = \alpha_d + \delta\alpha(T)$, to obtain

$$\Delta(T) = \alpha_d T + \left(\frac{\alpha_d^2}{\gamma F'[\alpha_d]} \right) T^{4-d}. \quad (98)$$

Thus in dimensions $d < 3$, we see that the dominant low temperature behavior is independent of γ , the strength of the mode-mode coupling, which enters into the subleading temperature dependence. At the marginal dimension $d = 3$, the linear coefficient of $\Delta(T)$ depends on γ , becoming independent of γ in the limit that $\gamma \rightarrow \infty$. We remark that here we are presenting

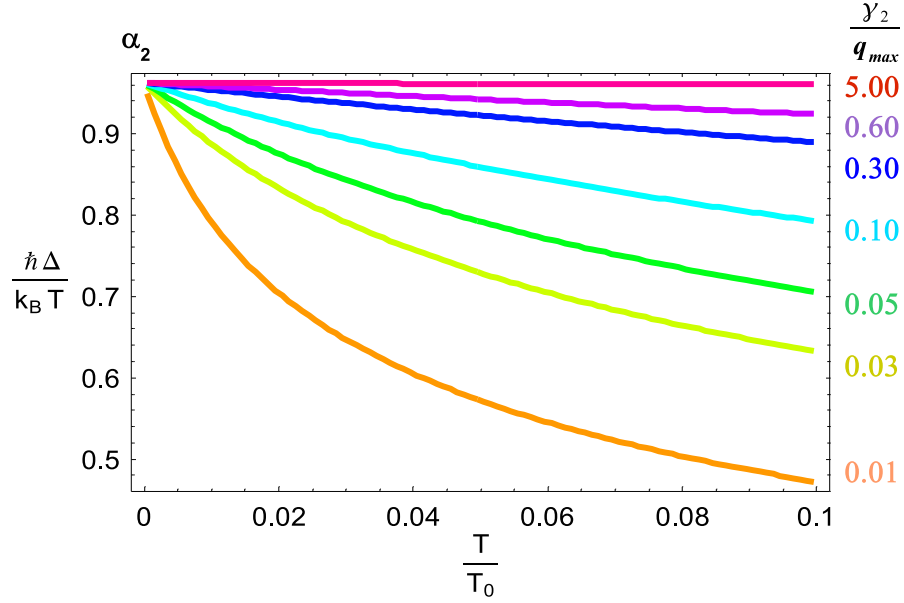


Figure 6: Temperature-dependence of Δ/T for $d = 2$ and coupling constants $\gamma_2 = 5.00, 0.60, 0.30, 0.10, 0.05, 0.03$ and 0.01 ; T_0 is the temperature scale where the correlation length and the lattice spacing are comparable ($\xi \sim a$).

and expanding a previous analysis²⁴, noting that the γ -independence of α for $d \leq 3$ can be understood via the insight that here temperature is a boundary effect in time.

In Figure 5 we display the dependence of α_d on dimensionality $1 < d < 3$. We notice that α_d goes to zero as the dimension approaches the lower critical dimension $d_c^l = 1$. α_d shows a maximum at $\alpha_{2.2} \approx 0.984$. We also present the $d = 2$ gap as a function of temperature for different coupling constants in Figure 6, noting that the y-intercepts remain the same, $\alpha_2 \approx 0.96$, in the limit of $T \rightarrow 0$. This value corresponds to the value of α_2 in Figure 5.

A similar plot for the $d = 3$ in Figure 7 indicates that α_3 is only independent of γ for large γ . According to (95) and (96), we write $\alpha_3^2 = \gamma F_3[\alpha]$ and solve for α_3 in the limit of upper cutoff $u_{max} = q_{max}/T \equiv 2\pi T_0/T \gg \alpha_3$,

$$\alpha_3(T, \gamma) \sim \sqrt{\frac{\gamma}{1 + \gamma(\frac{3}{8\pi^2}) \ln(\frac{4\pi T_0}{T})}}. \quad (99)$$

In the limit of strong coupling, $\alpha_3 \sim [\ln(\frac{4\pi T_0}{T})]^{-1/2}$ is γ independent. For weak coupling, the situation relevant here, α_3 is indeed a function of γ but remains independent of temperature so that $\Delta \sim T$ according to (93); temperature-dependences derived here should

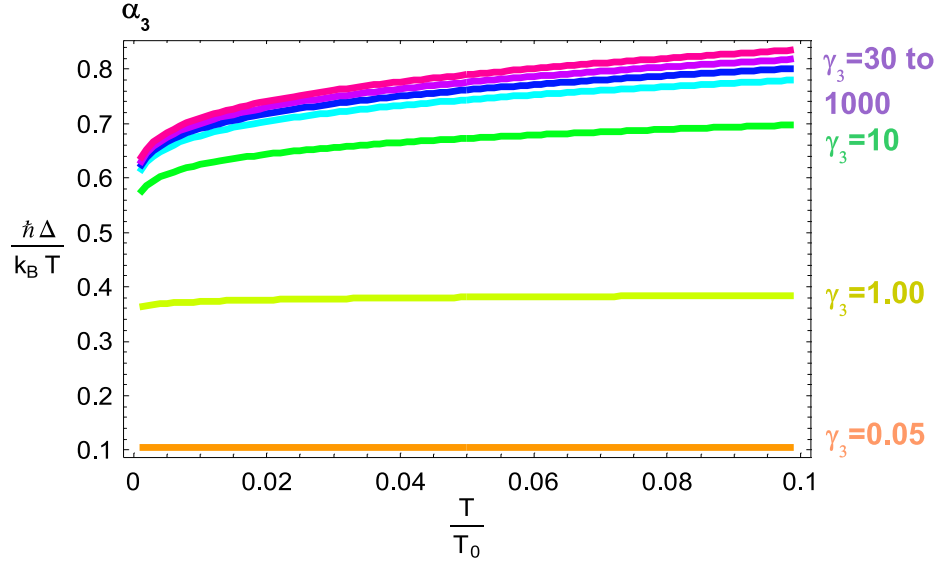


Figure 7: Temperature-dependence of Δ/T for $d = 3$ and coupling constants $\gamma_3 = 0.05, 1, 10$ and limiting large values $30 - 1000$; T_0 is the temperature where $\xi \sim a$.

therefore be in agreement with those found from a scaling perspective whenever direct comparison is possible.

C. Temperature-Dependent Dielectric Susceptibility

In order to test our self-consistent equations, we now use (89), and (91) to numerically determine the temperature-dependent paraelectric susceptibility in the approach to the quantum critical point (QCP) in $d = 3$; here we interchange QCP and QFCP freely since there are no other competing quantum critical points in this problem. We obtain $\chi^{-1}(T) = \Delta^2 \sim T^2$ for the approach $r = r_c$ in agreement with previous results and discussion. We note that a similar analysis in the vicinity of the classical phase transition leads to the expected Curie susceptibility ($\chi^{-1}(T \rightarrow T_c^+ \gg 0) \sim T$) since in this (high) temperature regime the Bose function in (92) scales as $\frac{T}{\omega}$. We also remark that if we assume that $\omega \equiv \omega_0$ with no q -dependence then we recover the Barrett⁴⁸ expression $\chi^{-1} \sim A + B \coth \frac{\hbar \omega_0}{k_B T}$; because the dispersion is constant and q -independent this approach is not applicable near quantum criticality where the gap vanishes and the q -dependence becomes important.

One more point needs to be considered before we proceed with our self-consistent mean-field theory (MFT). In the ordered ferroelectric phase the polarization field acquires a

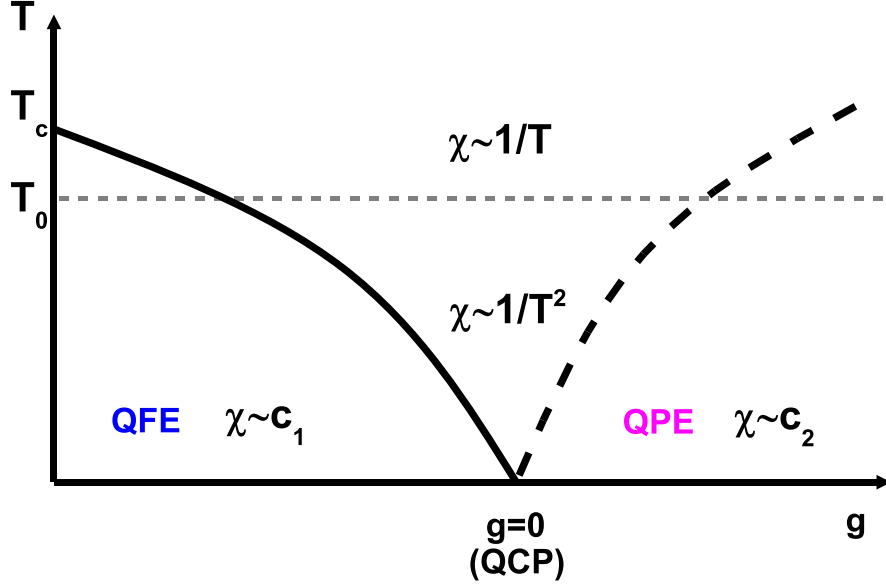


Figure 8: Schematic Phase Diagram indicating the Behavior of the Susceptibility as a Function of Temperature and Pressure; here T_c and T_0 are the Curie and the crossover ($\xi \sim a$) temperatures and $g = r - r_c$.

nonzero value. This equilibrium value P_0 enters the Lagrangian $\mathcal{L}_\mathcal{E}$ in (66) as $P = P_0 + \delta P$, where δP are fluctuations of the polarization field around its mean value, P_0 ($P_0 = 0$ in the paraelectric phase). The self energy (70) becomes

$$\Sigma = 3\gamma\langle P^2 \rangle = 3\gamma(P_0^2 + \langle \delta P^2 \rangle). \quad (100)$$

The equilibrium value P_0 is easily obtained by introducing an electric field into the Lagrangian by replacing $\mathcal{L}_\mathcal{E} \rightarrow \mathcal{L}_\mathcal{E} + E \cdot P$, then seeking the stationary point $\delta S/\delta P_0 = 0$ which gives

$$\langle rP_0 + 3\gamma\delta P^2 P_0 + \gamma P_0^3 - E \rangle = 0, \quad (101)$$

$$r + \Sigma - 2\gamma P_0^2 = \frac{E}{P_0} = 0 \quad (102)$$

at zero electric field. According to (83), $\Delta(r, T)^2 = r + \Sigma(r, T)$ so that the spectral gap in the ferroelectric phase is

$$\Delta_f(r, T)^2 = 2\gamma P_0(r, T)^2 > 0. \quad (103)$$

The crossover temperature, T_0 , between Curie ($\chi^{-1} \sim T$) and Quantum Critical ($\chi^{-1} \sim$

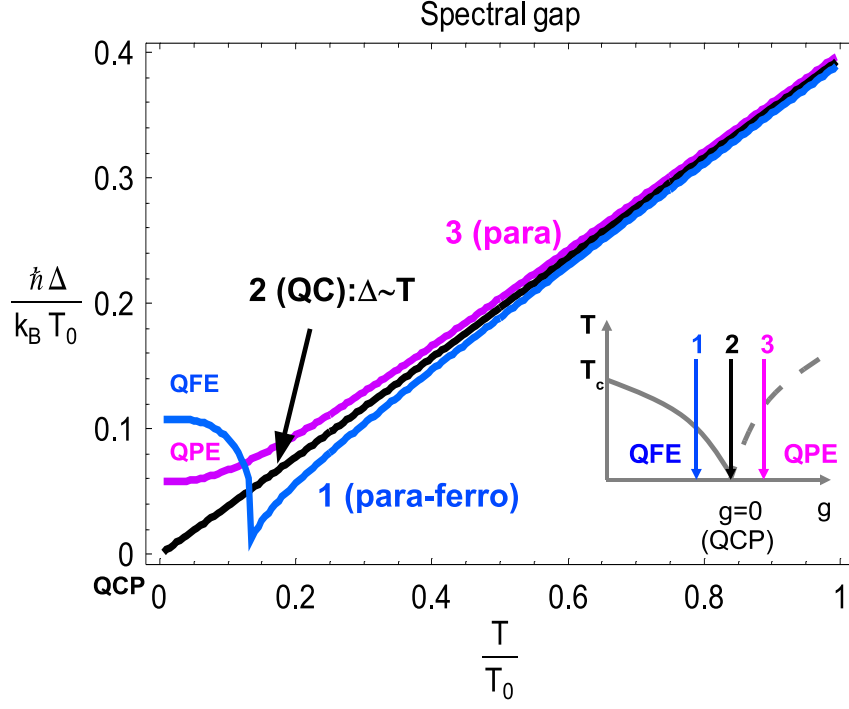


Figure 9: Temperature-dependence of the spectral gap for three temperature scans defined in the schematic inset; here $g = r - r_c$

T^2) behavior in the susceptibility is defined by the expression

$$T_0 \equiv \frac{\hbar c q_{max}}{2\pi k_B}, \quad (104)$$

which corresponds to the condition that the correlation length is comparable to the lattice constant ($\xi \sim a$); here the correlation length $\xi \equiv \frac{c}{\Omega_0} \sim g^{-1/2}$ (see (53)) and the momentum cutoff q_{max} is estimated to be the inverse lattice spacing (a^{-1}). For $SrTiO_3$, the sound velocity^{49,50} and the lattice constant¹⁴ have been measured to be $c = v_{STO} \approx 7900 m/s$ and $a_{STO} = 3.9 \times 10^{-10} m$ respectively; with these values, the crossover temperature is $T_0 \approx 23 K$. We note that with O^{18} substitution, the ambient pressure Curie temperature¹⁵ is $T_c \sim 24 K$. In Fig. 8 we present a schematic phase diagram based on these temperature scales for the expected behavior of the susceptibility; in particular we show that there is a finite phase region where the presence of the QCP has its influence on χ .

Experiments^{15,16} indicate that pressure (r) can tune a quantum paraelectric through a QCP into a quantum ferroelectric phase. In Fig. 9 we plot the calculated temperature-dependent spectral gap $\Delta(r, T)$ for three different pressure regimes as indicated in its

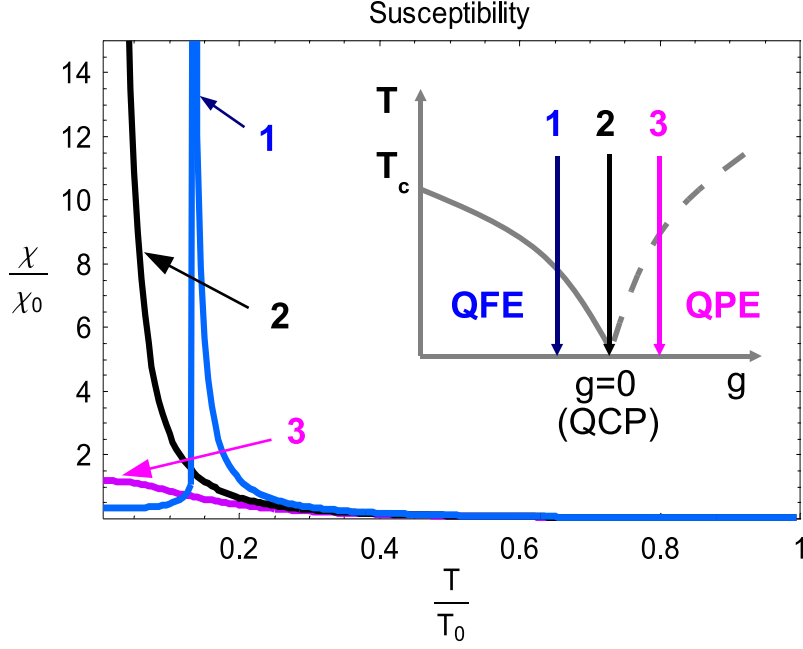


Figure 10: Temperature-dependence of the static dielectric susceptibility at low temperatures in three pressure regimes as defined in the inset; here $g = r - r_c$.

schematic inset. As expected, for (2) the spectral gap closes exactly at $T = 0$ leading to a linear dispersion relation, $\omega = q$ at the QCP. We note that in the quantum paraelectric (QPE), Δ (or χ^{-1}) is constant. In the quantum ferroelectric (QFE) again Δ is constant; though there exists a classical paraelectric-ferroelectric transition at $T = T_c$ where $\chi^{-1} \sim (T - T_c)$. The static dielectric susceptibility in the vicinity of the QCP (low T) is presented in the same three pressure regimes in Fig.10 where we see that in the QPE regime $\chi(T \rightarrow 0)$ saturates, at the QCP $\chi(T) \sim T^{-2}$ and diverges as $T \rightarrow 0$. In the QFE, the susceptibility also saturates at low temperatures, though the Curie law is recovered in the vicinity of the classical transition at $T = T_c$.

Next we present the calculated temperature-pressure phase diagram (Figure 11) that results from our SCMFT for the static dielectric susceptibility; here the power law exponents are depicted in different colors via the function $\frac{d \ln \chi^{-1}}{d \ln (T - T_c)/T_0}$. This expression selects the exponent 2 (blue region) for $\chi^{-1} \sim T^2$ ($T_c \equiv 0$ for QCP), exponent 1 (green region) for classical Curie behavior $\chi^{-1} \sim (T - T_c)$ and exponent 0 (red region) for a constant susceptibility. Once again we see in Figure 11 that, although the QCP exists strictly at zero temperature, it gives rise to a quadratic power law dependence of the inverse susceptibility on temperature

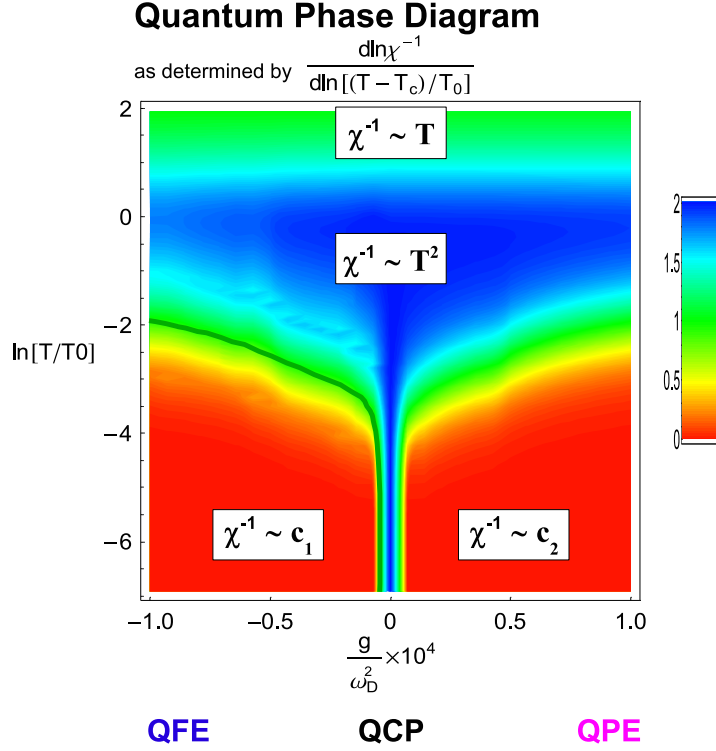


Figure 11: Temperature-Pressure (g) Phase Diagram as determined by a self-consistent analysis of the dielectric susceptibility; here $T_0 > T_c$ for all values of g .

(blue color in the plot) in a substantial region of the temperature-pressure (g) phase diagram; the crossover between quantum and classical behavior occurs at $\ln \frac{T}{T_0} \sim 0$ ($T \sim T_0$). We note that in Figure 11 $T_0 > T_c$ for all values of g so the region where $\chi^{-1} \sim T^2$ is larger than in Figure 8 where this is not the case.

Finally we note that in both Figs. 8 and 11, the x -axis refers to the tuning parameter difference $g = r - r_c$, (e.g. pressure or doping); we introduce the characteristic frequency scale $\omega_D = cq_{max}$ to introduce material-specific numbers into our plots. Using the values of c and $q_{max} \approx a_{STO}$ from above, we get $\omega_D \approx 2 \times 10^{13} Hz$ in $SrTiO_3$. The typical frequency $\Omega_0 = g^{1/2}$ (spectral gap at zero temperature) at which one observes the change of behavior in the dielectric susceptibility (blue region) is thus from Figure 11, $\Omega_0 \approx 10^{-2} \omega_D = 2 \times 10^{11} Hz$. Indeed, Raman scattering on ferroelectric $SrTi^{18}O_3$ ($T_c = 25K$) shows that the zero temperature Raman shift(ref.¹⁹). is about $10 cm^{-1}$ which translates into $\Omega_0 \approx 3 \times 10^{11} Hz$, in good agreement with our calculation. We note that the zero temperature QFE gap in Figure 9 also yields $\Delta_{T \rightarrow 0} = 0.1 \times \frac{k_B T_0}{\hbar} \approx 3.2 \times 10^{11} Hz$, indicating consistency between our

results and experiment.

Let us now look closely at the three pressure regimes discussed earlier, comparing Figures 10 and 11. In the (1) regime (Fig. 10), we start with a constant susceptibility in the QFE state at low temperatures (red region in Fig. 11). As T increases, we get to the classical ferroelectric-paraelectric transition at $T_c \gg 0$ (green region in Fig. 11; χ diverges in Fig. 10). By further increasing T , we go through a region influenced by the QCP (blue region; the so-called tornado effect) and later hit the classical high temperature regime at $T \approx T_0$ (green high temperature region in Fig. 11). The QC (2) regime with $g = 0$ ($r = r_c$) is simple; one sees $\chi^{-1} \sim T^2$ (blue region) at low temperatures that continuously changes to a classical Curie-type behavior (green region) at high temperatures. Finally the (3) regime in Fig. 10 starts with a constant susceptibility in the QPE state with $g > 0$ ($r > r_c$) at low temperatures (red region in Fig. 11), continues through a region of QCP influence (blue color) and ends up with a Curie-like behavior at high temperatures (green region). Notice that since the constant QPE behavior at low temperatures (red region, exponent 0) continuously changes to a QCP-influenced region (blue color, exponent 2), it must go through a (green) region of exponent 1, even though there is no phase transition (unlike the case of the QFE state). Fig. 11 thus displays the temperature-pressure (g) phase diagram for a paraelectric material with soft-mode dynamics based on our calculation of the dielectric susceptibility and graphically indicates the basin of attraction associated with the quantum critical point at finite temperatures. In a nutshell this ($T = 0$) quantum critical point has an influence in a region of the phase diagram at finite temperatures until $T \sim T_0$ ($\xi \sim a$) when the classical critical point dominates.

V. COUPLING TO LONG-WAVELENGTH ACOUSTIC MODES

A. Overview

Next we consider a coupling between the soft polarization and the long-wavelength acoustic (LA) phonon mode. Softening of the polar transverse optic (TO) mode near the QCP makes this coupling likely; in particular the gap closes entirely at the QCP (see Fig. 9). In this Section we introduce an additional coupling η between the TO polarization and the LA phonon modes into our SCMFT. We build upon our previous results; the coupling of

the polarization mode-mode interactions, γ , was already introduced in (22), (66) and (70). Using dimensional analysis (B), we show that both couplings are marginally relevant in the physically important dimension $d = 3$. We continue by deriving the gap equation (C) and study two distinct regions of the phase diagram: (i) in the QPE phase (D) (ii) in the vicinity of the QCP (E). In a nutshell, in this Section we show that within our SCMFT approach there exists a threshold η_c such that for $\eta > \eta_c$ a reentrant quantum ferroelectric phase emerges (F). We note that such a coupling to acoustic phonons has been considered previously²³ in the early days of the study of critical phenomena, and here we are rederiving and extending prior results in a contemporary framework.

B. Lagrangian and Dimensional Analysis

We introduce the coupling of the polarization ($P(\vec{x}, \tau)$) and the acoustic phonon ($\phi(\vec{x}, \tau)$) fields as a coupling of the polarization to strain $-\eta \nabla \phi P^2$; we then write the Lagrangian²³ as

$$\mathcal{L}_E[P, \phi] = \mathcal{L}_E[P] + \frac{m_a}{2} [(\partial_\tau \phi)^2 + c_a^2 (\nabla \phi)^2] - \eta \nabla \phi P^2, \quad (105)$$

where $\mathcal{L}_E[P]$ is our previous Lagrangian without acoustic coupling given in (66). Here the constant η is the coupling strength to the acoustic phonon; the latter's dynamics are introduced in the bracketed terms of (105).

We begin with a dimensional analysis of the couplings to assess their relative importance in the physically important dimension $d = 3$. In order to do so, we introduce the renormalization group (RG) flow by rescaling length, time, momentum and frequency

$$x' = \frac{x}{\Lambda}, \quad \tau' = \frac{\tau}{\Lambda}, \quad q' = q\Lambda, \quad \nu' = \nu\Lambda, \quad (106)$$

with constant $\Lambda > 1$ representing flow away from the infrared (IR) limit of the QCP, that is flow from small to large momentum and frequency. In terms of the rescaled variables x' and τ' , the action (68) with Lagrangian (105) in $d + 1$ dimensions becomes

$$\begin{aligned} S[P, \phi] &= \int_0^\beta d\tau \int d^d x \mathcal{L}_E[P, \phi] \\ &= \int_0^{\beta/\Lambda} d\tau' \int d^d x' \Lambda^{d+1} \left\{ \frac{1}{2} \Lambda^{-2} [(\partial_{\tau'} P)^2 + (\nabla' P)^2 + (\partial_{\tau'} \phi)^2 + (\nabla' c_a \phi)^2] \right. \\ &\quad \left. + \frac{1}{2} \Omega_0^2 P^2 + \frac{1}{4} \gamma P^4 - \eta \Lambda^{-1} \nabla' \phi P^2 \right\}. \end{aligned} \quad (107)$$

We emphasize that we write $\Omega_0^2 = r - r_c$ as the coefficient of the P^2 term in the Lagrangian $L_E[P]$ (66), entering (105) in (107), since our RG flow starts from the QCP ($r = r_c$). Rescaling P , ϕ , Ω_0^2 , γ and η , so that the action (107) assumes its initial form, we write

$$P' = P\Lambda^{\frac{d-1}{2}}, \quad (c_a\phi)' = (c_a\phi)\Lambda^{\frac{d-1}{2}}, \quad (\Omega_0^2)' = \Omega_0^2\Lambda^2, \quad \gamma' = \gamma\Lambda^{3-d}, \quad \eta' = \eta\Lambda^{2-\frac{d+1}{2}}, \quad (108)$$

which leads to

$$S[P, \phi] = \int_0^{\beta/\Lambda} d\tau' \int d^d x' \mathcal{L}_E[P', \phi']. \quad (109)$$

Now the fields, the mass term and the coupling constants flow to new values leaving the action unperturbed. We remark that the upper cutoff in the imaginary time dimension is replaced by infinity as the temperature $T \sim \frac{1}{\beta}$ approaches zero.

Analyzing the RG expressions in (108), we find that the Ω_0^2 term grows as we flow away from the QCP IR limit; therefore it is a relevant perturbation parameter independent of dimension d . This is consistent with the fact that $\Omega_0^2 = r - r_c = g$ tunes the system away from the QCP. Similarly we find that couplings γ and η grow (relevant) in dimension $d < 3$, decrease (irrelevant) in dimension $d > 3$, and don't change (marginally relevant) in $d = 3$. We see that in this case ($d = 3$) the coupling to acoustic phonons (η') is equally important as the mode-mode coupling (γ') and thus has to be included to the Gaussian model.

Let us now briefly summarize what we know about γ before we proceed to the discussion of the acoustic coupling η . In section IV B we found that the spectral gap Δ is independent of γ for dimensions $1 < d < 3$ in the zero temperature limit (see Fig. 6). This is in agreement with the above results, where γ is a relevant perturbative parameter; more precise analysis³ shows γ flowing to the nontrivial Wilson-Fisher fixed point γ^* . Here all the system properties become functions of $\gamma^* + \delta\gamma \approx \gamma^*$, and so are γ -independent. On the other hand, in dimensions $d > 3$ and $d = 3$, γ flows to zero (with logarithmic corrections in the marginal case). In these cases the system properties are functions of $\delta\gamma$ and thus are γ -dependent; we have already seen an example of this behavior in the specific case of the $d = 3$ spectral gap shown in Fig. 7.

C. Gap Equation

We are now ready to explore how the system's low-temperature behavior changes in the presence of acoustic phonons in the marginal (but physical) dimension $d = 3$. Let us look

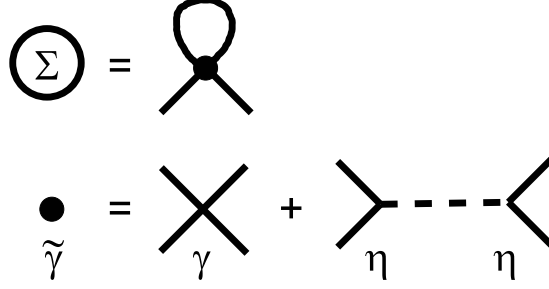


Figure 12: Diagrammatic representation of the self-energy that includes coupling to both optical and acoustic phonons.

first at the LA phonon field ϕ . Following the procedure of Section IV A, we find the acoustic Green's function and dispersion relation from (105) to be

$$D(q) \equiv D(\vec{q}, i\nu_n) = [(i\nu_n)^2 - c_a^2 q^2]^{-1}, \quad (110)$$

$$\omega_a(q) = c_a q \quad (111)$$

where, for simplicity, we absorb the effective crystal atomic mass m_a into a rescaling of the acoustic phonon field $\sqrt{m_a}\phi = \tilde{\phi}$, effectively setting it to 1.

We emphasize the P^2 -dependency of the new interaction term, $-\eta\nabla\phi P^2$, in the Lagrangian (105). Therefore it contributes to the polarization self-energy as an additional term inside the brackets of (72). This new contribution arises due to nonzero second-order perturbation and is schematically shown in Figure 12, where the solid line represents the soft polarization TO Green's function (81) and the dashed line represents the LA Green's function (110). We note that the interaction represented by a *dot* in the self-energy consists of a contribution each from the coupling γ and η . Thus we can write the polarization self-energy Σ as a sum of these two terms

$$\begin{aligned} \Sigma(r, T) &= \Sigma_\gamma(r, T) + \Sigma_\eta(r, T) \\ &= (-3\gamma)T \sum_n \int \frac{d^3q}{(2\pi)^3} G(q, i\nu_n) \\ &\quad + 4\eta^2 T \sum_n \int \frac{d^3q}{(2\pi)^3} q^2 G(q, i\nu_n) D(q, i\nu_n). \end{aligned} \quad (112)$$

where Σ_γ is the Hartree self-energy (86) previously calculated in Section IV A. We remark that the q^2 term in the integral for Σ_η arises due to form of the interaction $(\nabla\phi)$. Converting

the Matsubara summation to a contour integral, deformed around the poles $z_p = \pm\omega_p(q)$ and $z_a = \pm\omega_a(q)$ in the dispersion relations of the polarization (82) and acoustic phonon (111) modes respectively, we can rewrite Σ_η in the form²³

$$\Sigma_\eta(r, T) = -4\eta^2 \int \frac{d^3q}{(2\pi)^3} q^2 \left\{ \frac{[n(\omega_p(q)) + \frac{1}{2}]}{\omega_p[\omega_a^2 - \omega_p^2]} + \frac{[n(\omega_a(q)) + \frac{1}{2}]}{\omega_a[\omega_p^2 - \omega_a^2]} \right\}. \quad (113)$$

At the quantum critical point, where $r = r_c$ and $T = 0$, the dispersion $\omega_p(q) = q$ and $n(\omega_p) = n(\omega_a) = 0$ so that

$$\Sigma_\eta(r_c, 0) = -4\eta^2 \int \frac{d^3q}{(2\pi)^3} \frac{1}{2c_a(c_a + 1)q}. \quad (114)$$

Using (84), we write the gap function (as in IV A) as

$$\begin{aligned} \Delta^2 &= \Omega_0^2 + \Delta_\gamma^2 + \Delta_\eta^2, \\ \Delta_\gamma^2 &= 3\gamma \int \frac{d^3q}{(2\pi)^3} \left(\frac{[n(\omega_p(q)) + \frac{1}{2}]}{\omega_p} - \frac{1}{2q} \right), \\ \Delta_\eta^2 &= -4\eta^2 \int \frac{d^3q}{(2\pi)^3} q^2 \left(\frac{[n(\omega_p(q)) + \frac{1}{2}]}{\omega_p[\omega_a^2 - \omega_p^2]} + \frac{[n(\omega_a(q)) + \frac{1}{2}]}{\omega_a[\omega_p^2 - \omega_a^2]} - \frac{1}{2c_a[c_a + 1]q^3} \right), \end{aligned} \quad (115)$$

where Δ_γ^2 has been already defined in (89).

We emphasize that the γ and η terms in (115) have opposite signs in their contribution to the spectral gap Δ . The negative coefficient of η^2 reflects the fact that it emerges from second-order perturbation theory; physically it is due to thermally enhanced virtual excitations caused by coupling between polarization TO and LA phonon modes. Later in this Section we will see this negative sign is crucial in the interplay between the γ and η terms and gives rise to a possible first order transition at the QCP.

D. Deep in the Quantum Paraelectric Phase

Let us first explore the effect of the acoustic coupling η deep in the QPE region of the phase diagram (see inset of Figure 13). Here $g \gg 0$ and $\Delta \gg T \approx 0$. In this regime, we write

$$\chi^{-1} = \Delta^2 = \Omega_0^2 + D(\Delta) - A(\eta) \frac{T^4}{\Delta^2}, \quad (116)$$

with

$$A(\eta) = \frac{4\eta^2}{c_a} \int \frac{d^3u}{(2\pi)^3} u n(c_a u), \quad (117)$$

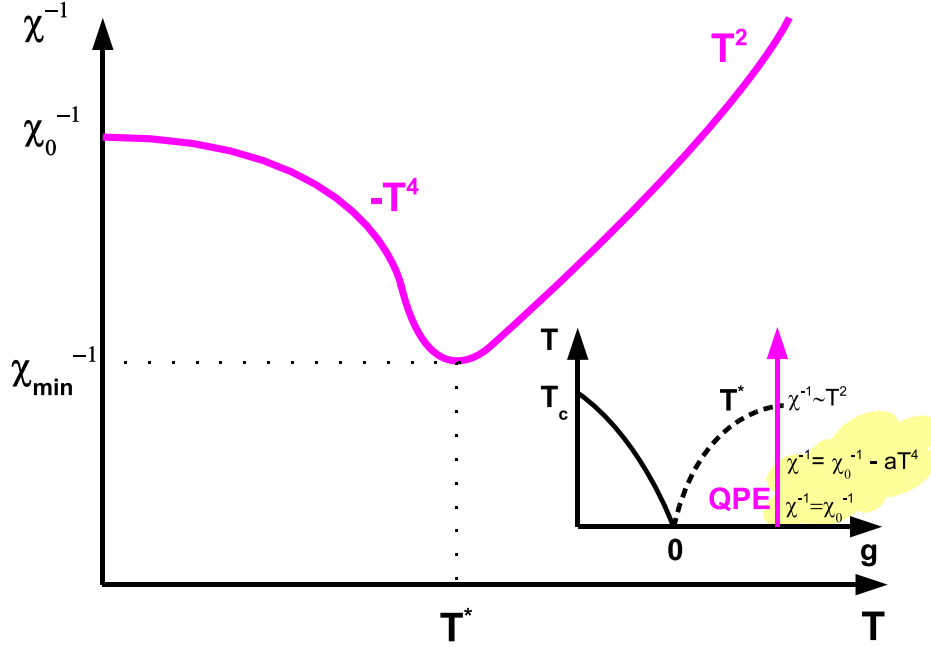


Figure 13: Temperature-dependence of the static dielectric susceptibility where coupling to a long-wavelength acoustic phonon is included in the calculation; inset indicates phase trajectory and region of corrections due to acoustic coupling deep in the QPE phase (yellow)

where derivations of $A(\eta)$ and $D(\Delta)$ are presented in Appendix A; for our purposes, the key point is to note that $\lim_{\Delta \rightarrow 0} D(\Delta) = 0$. Setting $A(\eta) \sim \eta^2 = 0$, we recover a constant expression for χ as a function of temperature in the QPE phase, consistent with our previous derivations from Section IV. For $\eta \neq 0$, the dielectric susceptibility acquires new low-temperature behavior. The quartic temperature term in (116), $-A(\eta) \frac{T^4}{\Delta^2}$, drives the inverse susceptibility at low temperatures; such a "bump" in the susceptibility (or "well" in the inverse susceptibility, see Fig. 13) due to acoustic phonon coupling has been considered previously²³. It is then natural to enquire whether a finite η could eventually drive the inverse susceptibility to zero (or negative) values. Here we show that this is not the case. We start by looking for a solution of (116) with $\chi^{-1} = \Delta^2 = 0$, and show that such a solution does not exist. Indeed at $\eta^2 = 0$, χ^{-1} in the QPE phase is nonzero as we saw in Section IV. At $\eta^2 \neq 0$, growth of last term in (116) exceeds all bounds and cannot equate a constant term Ω_0^2 (notice that $D(\Delta)|_{\Delta=0} = 0$). The inverse susceptibility therefore remains positive deep in the QPE phase with $\chi_{min}^{-1} \neq 0$.

We note that when the temperature increases so that $\Delta \sim T$ and we are no longer in the QPE phase (red in Fig. 11), we enter the "tornado" region of the QCP influence (blue in Fig. 11) where $\chi^{-1} \sim \Delta^2 \sim T^2$, as was shown in Section IV. At this point the quadratic temperature-dependence dominates and coupling to the acoustic phonons becomes negligible; as a result a turn-over in the inverse susceptibility from $-T^4$ to $+T^2$ -dependence occurs (see Fig. 13).

E. Quantum Critical Temperature-Dependent Dielectric Susceptibility

We already know that there exists a classical phase transition at T_c for $g < 0$ and $\eta = 0$; for $\eta \neq 0$ could this line of transitions enter the $g > 0$ part of the phase diagram and result in a reentrant quantum ferroelectric phase near the $g = 0$ QCP? In order to explore this possibility, we study the temperature-dependent susceptibility near the QCP (at $g = 0$) and find that unstable behavior is possible. Next we follow the line of transitions, where $\chi^{-1} = \Delta^2 = 0$ and show that its behavior is changed for $\eta > \eta_c$.

We begin with $\chi(T)$ in the vicinity in the quantum critical regime where $g = 0$ (trajectory 2 in Figure 10); here $\Omega_0^2 = g = 0$ and $q \sim \omega \sim T \gtrsim 0$ at low temperatures. Taking $\eta = 0$, the spectral gap (115) becomes

$$\Delta_\gamma^2 = \frac{3\gamma}{2\pi^2} \int dq q \frac{n(cq/T)}{c} \equiv \tilde{\alpha}\gamma T^2 \quad (118)$$

and we recover the quadratic temperature dependence, $\chi_\gamma^{-1} = \Delta_\gamma^2 \sim T^2$, that was derived in Section IV B.

With $\eta \neq 0$, the η contribution to the gap becomes

$$\Delta_\eta^2 = -\frac{4\eta^2}{2\pi^2} \int dq \frac{q}{c_a^2 - c^2} \left(\frac{n(cq/T)}{c} - \frac{n(c_a q/T)}{c_a} \right) \equiv -\tilde{\beta}\eta^2 T^2, \quad (119)$$

where c_a and $c = 1$ are the LA and (renormalized) TO sound velocities respectively. For both cases $c_a \leq c$, the expression under the integral in (119) is positive (see Appendix B for specifics), which results in a negative coefficient for Δ_η^2 . Adding both γ and η terms in the gap equation (115), we write the expression for the dielectric susceptibility

$$\chi^{-1} = \Delta^2 = \tilde{\gamma}T^2, \quad (120)$$

where

$$\tilde{\gamma} = f(\gamma) - g(\eta), \quad (121)$$

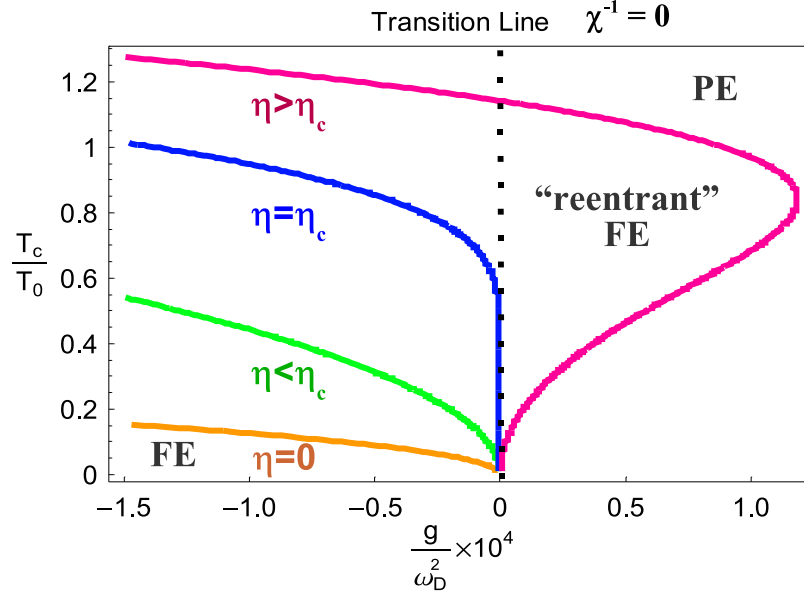


Figure 14: The transition line $T_c(g)$ for different values of η , the acoustic coupling constant; for $\eta > \eta_c$ indicating a first-order phase transition; the phase lines result from numerical solution of the gap equation ($\Delta(\eta \neq 0) = 0$) discussed in the text.

and

$$\begin{aligned} f(\gamma) &= \tilde{\alpha}\gamma, \\ g(\eta) &= \tilde{\beta}\eta^2. \end{aligned} \quad (122)$$

where $\tilde{\alpha}$ and $\tilde{\beta}$ are constants defined in (118) and (119) respectively and discussed in Appendix C. Here we see that the negative coefficient of $g(\eta)$ suggests the possibility of a negative (inverse) dielectric susceptibility, $\chi^{-1} \sim \tilde{\gamma} < 0$, and thus an instability near the ($g = 0$) QCP.

We define a critical value $\eta = \eta_c$ for which the inverse susceptibility goes to zero by setting

$$g(\eta_c) = f(\gamma). \quad (123)$$

For $\eta < \eta_c$, χ^{-1} is always positive and we may proceed as in Section IV, substituting $\tilde{\gamma}$ for γ . This way we include the acoustic coupling into a new effective constant $\tilde{\gamma}$, as is schematically depicted in Fig. 12. For $\eta > \eta_c$, there is new physics: the emergence of a reentrant (quantum) ferroelectric phase.

F. The Phase Transition Line $\chi^{-1} = 0$

We now study the phase transition line, defined by $\chi^{-1} = 0$ ($\Delta = 0$). From Section IV we know that there is a classical ferroelectric-paraelectric phase transtion at $g < 0$ at Curie temperature $T_c(g)$; it is depicted as a solid line in Fig. 8, where the dielectric susceptibility diverges, $\chi = \Delta^{-2} \rightarrow \infty$. Our results in Section IV are for $\eta = 0$, and we study the effect of $\eta > \eta_c > 0$ on this transition line.

To do this, we look for a solution to the gap equation (115), when $\Delta = 0$, which yields the transition line $T_c(g)$. When the spectral gap closes, the dispersion relations of the TO and the LA acoustic modes both become linear ($\omega_p(q) = cq$ and $\omega_a(q) = c_a q$). Plugging these values into (115) and setting $\Delta = 0$, we obtain

$$\begin{aligned} -2\pi^2\Omega_0^2 &= \frac{3\gamma}{c} \int_0^{q_{max}} dq q n(cq/T_c) - \frac{4\eta^2}{(c_a^2 - c^2)} \int_0^{q_{max}} dq q \left\{ \frac{n(cq/T_c)}{c} - \frac{n(c_a q/T_c)}{c_a} \right\} \\ &= T_c^2 \left\{ \frac{3\gamma}{c} \int_0^{u_{max}} du u n(cu) - \frac{4\eta^2}{(c_a^2 - c^2)} \int_0^{u_{max}} du u \left\{ \frac{n(cu)}{c} - \frac{n(c_a u)}{c_a} \right\} \right\} \end{aligned} \quad (124)$$

for the equation determining $T_c(g)$. At low temperatures, we note that we recover the scaling relation $\Omega_0^2 = g \sim T_c^2$ (60) since both integrals become proportional to T_c^2 ($u_{max} = \frac{q_{max}}{T_c} \gg 1$). At high temperatures $n(u) \approx \frac{1}{u}$, so the r.h.s. of (124) becomes proportional to T_c , and we recover the classical behavior $g \sim T_c$ (e.g. linear scaling between pressure and temperature).

The expression on the r.h.s. of (124) (divided by $2\pi^2$) is the same as the quantity $\tilde{\gamma}T_c^2$ introduced in the previous section (E). Near the transition line, we may therefore write

$$\chi^{-1} = \Omega_0^2 + \tilde{\gamma}T^2 \quad (125)$$

and we note that if we are in the $\Omega_0^2 = g > 0$ part of the T-g phase diagram, where no phase transition was present in the case of $\eta = 0$, a negative $\tilde{\gamma}$ may now drive the inverse susceptibility to an unstable region at high enough temperatures.

We solve (124) numerically and show the resulting plot of the $T_c(g)$ transition line in Figure 14; for the sake of completeness we note the parameters used here: $\gamma = c = 1, c_a = 0.9$, $\eta_c = 1.53$ and $\{\eta > \eta_c, \eta < \eta_c\} = \{1.59, 1.41\}$. We note that the x-axis scale is the same as in Fig(11), and we note that finite values of η shift the $T_c(g)$ line to a varying degrees. More specifically, for $\eta > \eta_c$, the transition line “wanders” into the $g > 0$ region, leading to a reentrant quantum ferroelectric phase. Such reentrance suggests the possibility of nearby coexistence and a line of first-order transitions ending in a tricritical point, but the

confirmation of this phase behavior requires a calculation beyond that presented here and will be the topic of future work.

VI. DISCUSSION

A. Logs, Dipolar Interactions and the Barrett Formula

Before summarizing our results, let us briefly touch on a number of topics closely related to our work which we have not yet discussed; more specifically they include logarithmic corrections in the upper critical dimension, dipolar interactions and the use of the Barrett formula for quantum paraelectrics. As we have already noted in Section VB, the polarization mode-mode interaction γ , and coupling to the acoustic phonons η , are both marginally relevant in the dimension of physical interest $d = 3$. Thus logarithmic corrections to the scaling relations (III) have to be included; we have already seen their appearance in the expression for α_3 in (99). The correction to scaling of the free energy near the classical ferro-paraelectric phase transition in four dimensions is³

$$f_{cl}(t, \gamma) = f_0(t, \gamma)[1 + 9\gamma \ln(t_0/t)]^{1/3}, \quad (126)$$

where $t = \frac{T-T_c}{T_c}$ is the reduced temperature, $f_0(t, \gamma) = t^2 \Phi\left(\frac{E/E_0}{|t/t_0|^{3/2}}\right)$ is the scaling form of the free energy with a universal scaling function Φ , $t_0 = O(1)$ and γ is the polarization mode-mode coupling at QCP. Since $\chi = \frac{\partial^2 f}{\partial E^2}|_{E=0}$, we have

$$\chi = \chi_0[1 + 9\gamma \ln(t_0/t)]^{1/3}, \quad (127)$$

where $\chi_0 \sim t^{-1}$. By applying the quantum-classical analogy (III), we write at the upper critical dimension, $d_c^u = 3$ ($d + z = 4$; $z = 1$),

$$f_{qm}(g, \gamma) = f_0(g, \gamma)[1 + 9\gamma \ln(g_0/g)]^{1/3}, \quad (128)$$

where $g_0 \equiv \omega_D^2 = O(1)$ is the Debye frequency squared, $f_0(g, \gamma)$ has the same form as before, and $g = \sigma(P - P_c)$ is the tuning parameter expressed as pressure difference with the electrostrictive constant σ . By setting $\chi = \frac{\partial^2 f}{\partial E^2}|_{E=0}$, the dielectric susceptibility becomes

$$\chi = \chi_0[1 + 9\gamma \ln(g_0/g)]^{1/3}, \quad (129)$$

where $\chi_0 \sim g^{-1} \sim T^{-2}$. The temperature-dependence of χ with logarithmic corrections is then found by making the substitution $g \sim T^2$ in (129), and these results are identical to those found previously using diagrammatic techniques²². An analogous procedure can be used to find the logarithmic corrections to other thermodynamic quantities.

We note that here we assume the upper critical (spatial) dimension $d_c^u = 3$; however if we include uniaxial dipole-dipole interactions, we will have $d_c^u = 2$. Basically this is because when all dipoles point in the (same) z -direction, the TO polarization frequency (82) becomes²⁰

$$\omega^2(q) = c^2 q^2 + \Delta^2 + \beta \frac{q_z^2}{q^2}, \quad (130)$$

where β is a constant, and we derive (130) in Appendix D. We note that the last term of (130) is specific to the uniaxial case. Applying simple scaling, we obtain

$$\tilde{q}_{x(y)} = \frac{q_{x(y)}}{b}, \quad \tilde{q}_z = \frac{q_z}{b^k}, \quad (131)$$

where the constants $b, b^k > 1$ represent flow to the infrared (IR) limit of the QCP. We show in Appendix D that in order for (130) and (131) to be satisfied simultaneously, k must equal 2 so that q_z “counts” for effectively *two* dimensions ($d_{eff}^{space} = d + 1$), so that for a quantum uniaxial ferroelectric the total effective dimension is $d_{eff} = d_{eff}^{space} + z = (d + 1) + z = d + 2$ with $d_c^u = 2$ since then we obtain $d_{eff} = 4$.

Though $SrTi^{18}O_3$ at high pressures and low temperature is most likely tetragonal, it is not clear if the samples are single-domain; hence the role of long-range dipolar interactions in these samples is still unknown. Similarly details of sample boundaries and possible depolarization fields resulting from surface charges are important for assessing the importance of such long-range dipolar forces. Finally the observed T^2 behavior of χ in the vicinity of the QCP suggests that dipolar interactions are not important (i.e. $d_{eff}^{space} = 3$); for $d_{eff}^{space} = 4$, a different T -dependence ($\chi^{-1} \sim T^3$) is expected²⁴ for a QPE so that a reexamination of the underlying model would be necessary to match experiment. Until details of the samples are known, this situation cannot be ascertained. We note that such T^2 dependence of the inverse susceptibility has also been observed⁴⁰ in mixed crystal ferroelectrics $KTa_{1-x}Nb_xO_3$ and $Ka_{1-y}Na_yTaO_3$ where uniaxial dipolar interactions are not important, and we encourage further low-temperature studies of these systems.

A consistent discrepancy between the observed low-temperature dielectric susceptibility and the Barrett formula⁴⁸ has been observed in the quantum paraelectric phase.^{9,40} Here we

emphasize that the discrepancy occurs when the system gets very close to the QCP; thus it provides a measure of the tuning distance to the QCP. Because the optical polarization mode softens as the system approaches the QCP, with the gap vanishing completely here, the momentum dependence in the dispersion relation (89) becomes important. It is exactly for this reason that the Barrett formula, that assumes a constant dispersion relation $\omega = \omega_0$, breaks down close to the QCP.

The Barrett formula works well deep in the QPE phase (Section V D), where the gap is much bigger than temperature. One such example is $KTaO_3$ (KTO), which remains paraelectric down to zero temperature, but in contrast to $SrTiO_3$ (STO) shows a much lower value of the zero temperature dielectric susceptibility ($\chi_{KTO} \approx 4000$, $\chi_{STO} \approx 24000$)^{9,51}. The closer the system is tuned to the QCP, the smaller is the spectral gap and the bigger is the dielectric susceptibility. Therefore, STO sits much closer to the QCP than KTO, and indeed KTO shows a nice fit to the Barrett formula⁵¹. Notice that by plugging ω_0 into (89), we get the Barrett expression⁴⁸,

$$\begin{aligned}\chi^{-1} = \Delta^2 &= \Omega_0^2 + \frac{3\gamma}{4\pi^2} \left(\frac{\coth(\omega_0/2T)}{\omega_0} \frac{q_{max}^3}{3} - \frac{q_{max}^2}{2} \right) \\ &= \frac{1}{M} \left(\frac{T_1}{2} \coth(T_1/2T) - T_0 \right),\end{aligned}\tag{132}$$

where $T_1 \equiv \omega_0$, and M and T_0 are fitting constants.

B. Summary and Open Questions

Let us now summarize the main results of the paper. Here our aim has been to characterize the finite-temperature properties of a material close to its quantum ferroelectric critical point; we have rederived and extended previous theoretical results using scaling methods and self-consistent mean-field theory. In the process we have made an analogy between temperature as a boundary effect in time and the Casimir effect, and have used this to shed light on both problems. Using simple finite-size scaling, we have presented straightforward derivations of finite-temperature observables for direct comparison with experiment, and our approach has yielded a scaling form $\chi(\omega) = \frac{1}{\omega} F(\frac{\omega}{T})$. We emphasize that this scaling method is useful in this system where z is low ($z = 1$); otherwise if z is higher, the system is usually well above its upper critical dimension where this approach is inappropriate. Next we've used self-consistent mean-field methods to determine the temperature-pressure (g) phase

diagram and the crossover between classical and quantum behavior. In particular we see the influence of the quantum critical point on the susceptibility at finite temperatures, and we can put in materials parameters to determine the size of its basin of attraction. Finally we include coupling to an acoustic phonon and find that it affects the transition line; for such couplings greater than a threshold strength there is a reentrant quantum ferroelectric phase.

Naturally these results suggest a number of open questions and here we list a few:

- The presence of a reentrant phase suggests the possibility of nearby phase coexistence, a tricritical point and a line of first order transitions. This is a particularly appealing scenario given recent experiments⁵² suggesting coexistence of QPE and QFE in $SrTi^{18}O_3$ and is a topic we plan to pursue shortly.
- If indeed there is a tricritical point and a line of first-order phase transitions, could there also be a metaelectric critical point in the $g - E$ plane analogous to the metamagnetic situation^{53,54} in some metallic systems? There is indication that an analogous metaelectric critical point occurs in a multiferroic system,⁵⁵ so this is a question driven by recent experiment.
- What happens when we add spins to a system near its quantum ferroelectric critical point? Would the resulting multiferroic have particularly distinctive properties?
- Similarly what type of behavior do we expect if we dope a quantum paraelectric in the vicinity of a QCP? There is by now an extensive body evidence that electronically mediated superconductivity is driven by the vicinity to a magnetic quantum critical point, phenomenon of "avoided criticality", whereby superconductivity in the vicinity of a naked magnetic quantum critical point^{56,57}. In such systems, the metallic transport properties develop strange metallic properties that have been termed "non-Fermi liquid behavior"^{58,59}. This raises the important question, as to what, if any, is the ferroelectric counterpart to this behavior? In particular - how does the presence of a soft mode affect the semi-metallic properties of a doped quantum critical ferro-electric, and does a doped ferroelectric quantum critical point also develop superconductivity via the mechanism of avoided criticality?

We believe that we have only begun to explore the rich physics associated with the quantum ferroelectric critical point, a simple setting for studying many issues associated with quantum criticality that emerge in much more complex materials. Furthermore the possibility of detailed interplay between theory and experiment is very encouraging.

VII. ACKNOWLEDGMENTS

We thank D. Khmel'nitskii, G.G. Lonzarich, S.E. Rowley, S.S. Saxena and J.F. Scott for detailed discussions. We also acknowledge financial support from the National Science Foundation nsf-dmr 0645461 (L.Palova), NSF-NIRT-ECS-0608842 (P. Chandra) and the Department of Energy, grant DE-FE02-00ER45790 (P. Coleman).

VIII. APPENDIX A: $D(\Delta)$ AND $A(\eta)$

We derive expressions for $D(\Delta)$ and $A(\eta)$ (117) using the gap equation (115) deep in the QPE region (D), where $g \gg 0$ and $\Delta \gg T \approx 0$. Collecting all “ $\frac{1}{2}$ ”-terms under integrals of Δ_γ^2 and Δ_η^2 in (115), we obtain the expression for $D(\Delta)$,

$$\begin{aligned}
D(\Delta) &\equiv \frac{3}{2}\gamma \int \frac{d^3q}{(2\pi)^3} \left(\frac{1}{\omega_p} - \frac{1}{q} \right) - 2\eta^2 \int \frac{d^3q}{(2\pi)^3} q^2 \left(\frac{1}{\omega_a[\omega_p^2 - \omega_a^2]} - \frac{1}{q^3 c_a[c^2 - c_a^2]} \right) \\
&\quad - 2\eta^2 \int \frac{d^3q}{(2\pi)^3} q^2 \left(\frac{1}{\omega_p[\omega_a^2 - \omega_p^2]} - \frac{1}{q^3 c[c_a^2 - c^2]} \right) \equiv \frac{3\gamma}{4\pi^2} I_1 - \frac{\eta^2}{c_a \pi^2} I_2 - \frac{\eta^2}{\pi^2} I_3, \\
I_1 &= \int_0^{q_{max}} dq q^2 \left(\frac{1}{\sqrt{\Delta^2 + q^2}} - \frac{1}{q} \right), \\
I_2 &= \int_0^{q_{max}} dq q^3 \left(\frac{1}{\Delta^2 + q^2[c^2 - c_a^2]} - \frac{1}{q^2[c^2 - c_a^2]} \right), \\
I_3 &= \int_0^{q_{max}} dq q^4 \left(\frac{1}{\sqrt{\Delta^2 + c^2 q^2}[-\Delta^2 + q^2[c_a^2 - c^2]]} - \frac{1}{q^3 c[c_a^2 - c^2]} \right). \tag{133}
\end{aligned}$$

Notice that $\lim_{\Delta \rightarrow 0} D(\Delta) = 0$, since all three integrals I_1 , I_2 and I_3 become zero at zero gap. We split the integrals I_i ($i = 1, 2, 3$) into two parts, $I_i = \int_0^{n\Delta} + \int_{n\Delta}^{q_{max}}$, where $n\Delta \gg \Delta$. Since $q \gg \Delta$ in the second integral part, we neglect its Δ dependence and get a zero contribution. Thus, only the first integral part contributes, and $D(\Delta)$ becomes a function of Δ only with no temperature dependence.

Next we show that the second Bose-Einstein $n(\omega_a(q))$ term under the integral of Δ_η^2 in

(115) results in the form $A(\eta)$ in equation (117),

$$\begin{aligned} -4\eta^2 \int \frac{d^3q}{(2\pi)^3} q^2 \frac{n(\omega_a(q))}{\omega_a[\omega_p^2 - \omega_a^2]} &= -4\eta^2 \int \frac{d^3q}{(2\pi)^3} q^2 \frac{n(\omega_a(q))}{c_a q [\Delta^2 + q^2(c^2 - c_a^2)]} \\ &\approx -\frac{4\eta^2}{c_a} \frac{T^4}{\Delta^2} \int \frac{d^3u}{(2\pi)^3} u n(c_a u) \equiv -A(\eta) \frac{T^4}{\Delta^2}, \end{aligned} \quad (134)$$

where $u = q/T$. Notice that we approximate $\Delta^2 \gg q^2(c^2 - c_a^2)$ in the second line of (134). For low momenta, this is indeed true. For large momenta $q \gg \Delta \gg T \approx 0$, we neglect Δ in (134) and the integral becomes

$$-\frac{4\eta^2}{2\pi^2 c_a (c^2 - c_a^2)} \int dq q n(c_a q). \quad (135)$$

In the limit $q \gg T$, $n(c_a q) \approx e^{-c_a q/T}$ and (135) becomes exponentially small ($\sim T^2 e^{-c_a q/T}$) and can be neglected. Similarly, we neglect the rest of the terms in the gap function (115) with Bose-Einstein thermal distribution $n(\omega_p(q))$. Deep in the QPE phase $\Delta \gg T$, so that $n(\omega_p(q)) \approx e^{-\Delta/T}$ at low momenta or $n(\omega_p(q)) \approx e^{-cq_{large}/T}$ at large momenta. In both cases $\Delta, q_{large} \gg T$, the integrals containing $n(\omega_p(q))$ become exponentially small and so are negligible.

IX. APPENDIX B: INTEGRAL (119) IS POSITIVE FOR $c_a \leq c$

We also show that the expression under the integral in (119) is positive for the two cases, $c_a \leq c$. First, assuming that $c_a < c$, $c_a q < cq$ (for positive q 's) and $n(c_a q/T) > n(cq/T)$ we write

$$\begin{aligned} \left\{ \frac{n(cq/T)}{c} - \frac{n(c_a q/T)}{c_a} \right\} \frac{1}{c_a^2 - c^2} &> \left(\frac{1}{c} - \frac{1}{c_a} \right) n(c_a q/T) \frac{1}{c_a^2 - c^2} \\ &= \frac{1}{cc_a(c_a + c)} n(c_a q/T) \geq 0, \end{aligned} \quad (136)$$

which we note is positive. Similarly, for $c_a > c$, $c_a q > cq$ and $n(c_a q/T) < n(cq/T)$, we write

$$\begin{aligned} \left\{ \frac{n(cq/T)}{c} - \frac{n(c_a q/T)}{c_a} \right\} \frac{1}{c_a^2 - c^2} &> \left(\frac{1}{c} - \frac{1}{c_a} \right) n(cq/T) \frac{1}{c_a^2 - c^2} \\ &= \frac{1}{cc_a(c_a + c)} n(cq/T) \geq 0. \end{aligned} \quad (137)$$

which is also positive. Therefore the integral in (119) is positive in both cases.

X. APPENDIX C: $\tilde{\alpha}$ AND $\tilde{\beta}$ ARE CONSTANTS

To evaluate the quantities $\tilde{\alpha}$ and $\tilde{\beta}$ in (118) and (119), we make a change of variables $u = cq/T$, and $u = c_a q/T$. The expressions for these two constants then become

$$\begin{aligned}\tilde{\alpha} &= \frac{3}{2\pi^2 c^3} \int_0^{cq_{max}/T} du u n(u) = \frac{1}{4c^3} \\ \tilde{\beta} &= \frac{2}{\pi^2(c_a^2 - c^2)} \left[\frac{1}{c^3} \int_0^{cq_{max}/T} - \frac{1}{c_a^3} \int_0^{c_a q_{max}/T} \right] du u n(u) = \frac{1}{3(c_a^2 - c^2)} \left(\frac{1}{c^3} - \frac{1}{c_a^3} \right).\end{aligned}\quad (138)$$

where we have taken the limits of integration to infinity and used the result $\int_0^\infty du u n(u) = \frac{\pi^2}{6}$.

XI. APPENDIX D: DIPOLE-DIPOLE INTERACTIONS IN UNIAXIAL FERRO-ELECTRICS

Interaction energy between two dipoles \vec{p}_i and \vec{p}_j sitting on two sites \vec{r}_i and \vec{r}_j respectively is

$$W_{ij}(\vec{r}) = \frac{\vec{p}_i \cdot \vec{p}_j - 3(\vec{n} \cdot \vec{p}_i)(\vec{n} \cdot \vec{p}_j)}{4\pi\epsilon_0|\vec{r}|^3}, \quad (139)$$

where \vec{n} is a unit vector in the direction of the vector $\vec{r} \equiv \vec{r}_j - \vec{r}_i$. From (139), we find the total dipole-dipole interaction potential,

$$W(\vec{r}) = \frac{1}{4\pi\epsilon_0} \sum_{i,j,a,b} p_i^a p_j^b \left(\frac{\delta_{ab}}{r^3} - \frac{3r^a r^b}{r^5} \right), \quad (140)$$

where $r \equiv |\vec{r}|$, and a, b label vector coordinates. After Fourier transform, the interaction potential becomes,

$$W(\vec{q}) = \frac{1}{\epsilon_0} \sum_{a,b} p_{\vec{q}}^a p_{-\vec{q}}^b \frac{q_a q_b}{q^2}, \quad (141)$$

where $q \equiv |\vec{q}|$ is momentum dependence of $W(\vec{q})$. Assuming that all dipoles point in the same(z)-direction in the uniaxial case, the dipole potential becomes proportional to,

$$W(\vec{q}) \sim \frac{q_z^2}{q^2}. \quad (142)$$

$W(\vec{q})$ contributes to Lagrangian (105), $L_E[P, \Phi] \rightarrow L_E[P, \Phi] + W$, so the TO polarization frequency (82) reads²⁰

$$\omega^2(q) = c^2 q^2 + \Delta^2 + \beta \frac{q_z^2}{q^2}, \quad (143)$$

where we introduce constant of proportionality β .

We show that (130) and (131) conditon $k = 2$. Let us assume that $k > 1$. Then,

$$\begin{aligned}\tilde{q}^2 &= \tilde{q}_x^2 + \tilde{q}_y^2 + \tilde{q}_z^2 = \frac{q_x^2 + q_y^2}{b^2} + \frac{q_z^2}{(b^2)^k} \approx \frac{q^2}{b^2}, \\ \frac{\tilde{q}_z^2}{\tilde{q}^2} &\approx b^{2-2k} \frac{q_z^2}{q^2}.\end{aligned}\tag{144}$$

Since we also rescale frequency $\omega(q)$ (130) by a constant, expressions, \tilde{q}^2 and $\frac{\tilde{q}_z^2}{\tilde{q}^2}$, are to be proportional. This leads then to the condition,

$$k = 2.\tag{145}$$

-
- ¹ H.B.G. Casimir, “On the attraction between two perfectly conducting place,” H.B. G. Casimir, *Proc. Kon. Ned. Akad. Wetenschap* **51**, 793 (1948); H.B.G. Casimir and D. Polder, “The Influence of Retardation on the London-van der Waals Forces,” *Phys. Rev.* **73**, 360 (1948).
 - ² H.B. Chan, V.A. Aksyuk, R.N. Kleiman, D.J. Bishop, F. Capasso,” Quantum Mechanical Actuation of Micromechanical Systems by the Casimir Force,” *Science* **291**, 1941 (2001).
 - ³ J. Cardy, *Scaling and Renormalization In Statistical Physics*, (Cambridge University Press, Cambridge, 1999).
 - ⁴ S.L. Sondhi, S.M. Girvan, J.P. Carini and D. Shahar, “Continuous Quantum Phase Transitions,” *Rev. Mod. Phys* **69**, 315 (1997).
 - ⁵ S. Sachdev, *Quantum Phase Transitions*, (Cambridge University Press, Cambridge 1999).
 - ⁶ P. Coleman and A.J. Schofield, “Quantum Criticality,” *Nature* **433**, 226 (2005).
 - ⁷ W.G. Unruh, “Notes on black hole evaporation,” *Phys. Rev. D* **14**, 870 (1076).
 - ⁸ K. Thorne, *Black Holes amd Time Warps: Einstein’s Outgrageous Legacy*, (W.W. Norton anc Co, 1995)
 - ⁹ K.A. Muller and H. Burkard, “*SrTiO*₃: An intrinsic quantum paraelectric below 4 K”, *Phys. Rev. B* **19**, 3593 (1979).
 - ¹⁰ M. Itoh, R. Wang, Y. Inaguma, T. Yamamguchi, Y-J. Shan, and T. Nakamura, “Ferroelectricity Induced by Oxygen Isotope Exchange in Strontium Titanate Perovskite,” *Phys. Rev. Let.* **82**, 3540 (1999).
 - ¹¹ W. Zhong and D. Vanderbilt, “Competing Structural Instabilities in Cubic Perovskites,” *Phys. Rev. Lett.* **74**, 2587 (1995); W. Zhong and D. Vanderbilt, “Effect of Quantum Fluctuations on Structural Phase Transitions in *SrTiO*₃ and *BaTiO*₃,” *Phys. Rev. B* **53**, 5047 (1996).

- ¹² N.Sai and D. Vanderbilt, “First-Principles Study of Ferroelectric and Antiferrodistortive Instabilities in Tetragonal $SrTiO_3$,” *Phys. Rev. B* **62**, 13942 (2000).
- ¹³ H. Uwe and T. Sakudo, “Stress-induced ferroelectricity and soft phonon modes in $SrTiO_3$,” *Phys. Rev. B* **13**, 271 (1976).
- ¹⁴ J.H. Haeni, P. Irvin, W. Chang, R. Uecker, P. Reiche, Y.L. Li, S. Choudhury, W. Tian, M.E. Hawley, B. Craigo, A.K. Tagantsev, X.Q. Pan, S.K. Streiffer, L.Q. Chen, S.W. Kirchoefer, J. Levy and D.G. Schlom,”Room-temperature ferroelectricity in strained $SrTiO_3$, *Nature* **430**, 758 (2004).
- ¹⁵ E.L. Venturini, G.A. Samara, M. Itoh and R. Wang, “Pressure as a probe of the physics of ^{18}O -substituted $SrTiO_3$,” *Phys. Rev. B* **69**, 184105 (2004).
- ¹⁶ P. Coleman, “Theory Perspective: SCES 05 Vienna,” *Physica B* **378-380**, 1160 (2006); S.E. Rowley et al., unpublished.
- ¹⁷ D.E. Grupp and A.M. Goldman, “Giant Piezoelectric Effect in Strontium Titanate at Cryogenic Temperatures,” *Science* **276**, 382 (1997).
- ¹⁸ S. Horiuchi, Y. Okimoto, R. Kumai and Y. Tokura, “Quantum Phase Transition in Organic Charge-Transfer Complexes,” *Science* **299**, 229 (2003).
- ¹⁹ M. Takesada, M. Itoh and T. Yagi, “Perfect Softening of the Ferroelectric Mode in the Isotope-Exchanged Strontium Titanate of $SrTi^{18}O_3$ Studied by Light Scattering,” *Phys. Rev. Lett.* **96**, 227602 (2006).
- ²⁰ A.I. Larkin and D.E. Khmel’nitskii, “Phase Transition in Uniaxial Ferroelectrics,” *Sov. Phys. JETP* **29**, 1123 (1969).
- ²¹ G. Ahlers, A. Kornblit and H.J. Guggenheim, “Logarithmic Corrections to the Landau Specific Heat near the Curie Temperature of the Dipolar Ising Ferromagnet $LiTbF_4$,” *Phys. Rev. Lett.* **34**, 1227 (1975); G. Ahlers, “Critical Phenomena at Low Temperature,” *Rev. Mod. Phys.* **52**, 489 (1980).
- ²² A.B. Rechester, “Contribution to the Theory of Second-Order Phase Transitions at Low Temperatures,” *Sov. Phys. JETP* **33**, 423 (1971).
- ²³ D.E. Khmel’nitskii and V.L. Shneerson, “Low-Temperature Displacement-Type Phase Transition in Crystals,” *Sov. Phys.- Solid State* **13**, 687 (1971); *ibid Sov. Phys. JETP* **37**, 164 (1973).
- ²⁴ T. Schneider, H. Beck, and E. Stoll, “Quantum effects in an n-component vector model for structural phase transitions,” *Phys. Rev. B* **13**, 1123 (1976).
- ²⁵ D. Schmeltzer, “Quantum Ferroelectric: A Renormalization-Group Study,” *Phys. Rev. B* **27**, 459 (1983).
- ²⁶ R. Roussev and A.J. Millis, “Theory of the quantum paraelectric-ferroelectric transition,” *Phys. Rev. B* **67**, 014105 (2003).

- ²⁷ N. Das and S.G. Mishra, “Fluctuations and Criticality in Quantum Paraelectrics,” cond-mat arXiv:0707.2634.
- ²⁸ S.E. Rowley, L.J. Spalek and S.S. Saxena, “Quantum Criticality in Ferroelectricity”, submitted; S.E. Rowley and S.S. Saxena, private communication.
- ²⁹ S.K. Lamoreaux, “Demonstration of the Casimir force on the 0.6 to 6 μm range,” *Phys. Rev. Lett.* **78**, 5 (1997).
- ³⁰ U. Mohideen and A. Roy, “Precision measurement of the Casimir force from 0.1 to 0.9 μm ,” *Phys. Rev. Lett.* **81**, 4549 (1998).
- ³¹ M. Lisanti, D. Iannuzzi and F. Capasso, “Observation of the skin-depth effect on the Casimir force between metallic surfaces,” *PNAS* **102**, 11989 (2005).
- ³² J.M. Obrecht, R.J. Wild, M. Antezza, L.P. Pitaevskii, S. Stringari and E.A. Cornell, “Measurement of the Temperature-Dependence of the Casimir-Polder Force,” *Phys. Rev. Lett.* **98**, 062301-1-4 (2007).
- ³³ G.D. Mahan, *Many-Particle Physics* (Plenum Press, New York, 1981).
- ³⁴ E. Lifshitz, *Sov. Phys. JETP* **2**, 73 (1956).
- ³⁵ F.J. Belinfante, “The Casimir Effect Revisited,” *Am. J. Phys.* **55**, 134 (1987).
- ³⁶ E. Elizalde and A. Romeo, “Essentials of the Casimir Effect and its Computation,” *Am. J. Phys.* **59**, 711 (1991).
- ³⁷ D.L. Andrews and L.C. Davila Romero, “Conceptualization of the Casimir Effect,” *Eur. J. Phys.* **22**, 447-451 (2001).
- ³⁸ S.L. Boersma, “A maritime analogy of the Casimir effect,” *Am. J. Phys.* **64**, 539-541 (1996).
- ³⁹ J. Hertz, “Quantum Critical Phenomena” *Phys. Rev. B* **14**, 1165 (1976).
- ⁴⁰ D. Rytz, U.T. Hochli and H. Bilz, “Dielectric Susceptibility in Quantum Ferroelectrics,” *Phys. Rev. B* **22**, 359 (1980).
- ⁴¹ J. Schwinger, “On Gauge Invariance and Vacuum Polarization,” *Phys. Rev.* **82**, 664 (1951); J. Schwinger, “Casimir Effect in Source Theory II,” *Lett. Math. Phys.* **24**, 59 (1992).
- ⁴² , S.K. Lamoreaux, “Resource Letter CF-1: Casimir Force,” *Am. J. Phys.* **67**, 850 (1999).
- ⁴³ L.D. Landau and E. M. Lifshitz, “Statistical Physics” 3rd Edition Part 1 *Course of Theoretical Physics* Volume **5** (1975).
- ⁴⁴ M.E. Lines and A.M. Glass, *Principles and Applications of Ferroelectrics and Related Materials*, (Oxford University Press, Oxford, 1977).
- ⁴⁵ R. Wang and M. Itoh, “Suppression of the quantum fluctuation in ^{18}O -enriched strontium

- titanate,” *Phys. Rev. B* **64**, 174104 (2001).
- ⁴⁶ M.C. Aronson, R. Osborn, R.A. Robinson, J.W. Lynn, R. Chau, C.L. Seaman, and M.B. Maple, *Phys. Rev. Lett.* **75**, 725 (1995).
- ⁴⁷ A. Schroeder *et al.*, *Nature* **407**, 351(2000).
- ⁴⁸ J.H. Barrett, *Phys. Rev.* **86**, 118 (1952).
- ⁴⁹ C. v. K. Schmising et al., “Strain Propagation in Nanolayered Perovskites Probed by Ultrafast X-Ray Diffraction,” *Phys. Rev. B* **73**, 212202 (2006).
- ⁵⁰ R.O. Bell and G. Rupprecht, “Elastic Constants of Strontium Titanate,” *Phys. Rev.* **129**, 90 (1963).
- ⁵¹ A. R. Akbarzadeh, L. Bellaiche, K. Leung, J. Iniguez, and D. Vanderbilt, “Atomistic simulations of the incipient ferroelectric $KTaO_3$,” *Phys. Rev. B* **70**, 054103 (2004).
- ⁵² H. Taniguchi and M. Itoh, *Phys. Rev. Lett.* **99** 017602 (2007).
- ⁵³ A.J. Millis, A.J. Schofield, G.G. Lonzarich and S.A. Grigera, “Metamagnetic Quantum Criticality,” *Phys. Rev. Lett.* **88** 217204 (2002).
- ⁵⁴ P. Gegenwart, Q. Si and F. Steglich, “Quantum Criticality in Heavy-Fermion Metals,” *Nature* **4**, 186 (2008).
- ⁵⁵ J.W. Kim et al., “Dielectric Constant Increase near the Magnetic-Field Induced Metaelectric Transition in Multiferroic $BiMn_2O_5$,” submitted to *Nature Physics*.
- ⁵⁶ N. D. Mathur, F. M. Grosche, S. R. Julian, I. R. Walker, D. M. Freye, R. K. W. Haselwimmer, and G. G. Lonzarich, “Magnetically mediated superconductivity in heavy fermion compounds”, *Nature*, 394, 39 (1998).
- ⁵⁷ B. Laughlin, G. G. Lonzarich, P. Monthoux, and D. Pines, “The quantum criticality conundrum”, *Adv. Phys.* 50, 361 (2001).
- ⁵⁸ P. Coleman, C. Pepin, Q. Si, and R. Ramazashvili, “How do Fermi liquids get heavy and die?”, *J. Phys.: Condens. Matter* **13**, 723(R) (2001).
- ⁵⁹ H. von Löhneysen, A. Rosch, M. Vojta, M., and P. Wolfe, “Fermi-liquid instabilities at magnetic quantum phase transitions”. *Rev. Mod. Phys.* 79, 1015 (2007) and references therein.